We are IntechOpen,
the world's leading publisher of
Open Access books
Built by scientists, for scientists

4,800
Open access books available

122,000
International authors and editors

135M
Downloads

Our authors are among the

154
Countries delivered to

TOP 1%
most cited scientists

12.2%
Contributors from top 500 universities

CLARIVATE ANALYTICS

BOOK CITATION INDEX

INDEXED

WEB OF SCIENCE™

Selection of our books indexed in the Book Citation Index
in Web of Science™ Core Collection (BKCI)

Interested in publishing with us?
Contact book.department@intechopen.com

Numbers displayed above are based on latest data collected.
For more information visit www.intechopen.com

Photonic Crystal Multiplexer/Demultiplexer Device for Optical Communications

Sahbuddin Shaari[1] and Azliza J. M. Adnan[2]

[1]*Universiti Kebangsaan Malaysia, Bangi, Selangor,*
[2]*Telekom Reserach & Development Sdn. Bhd, Cyberjaya,*
Malaysia

1. Introduction

Photonic crystals (PhCs) are periodic dielectric structures. They are called *crystals* because of their periodicity and *photonic* because they act on light. They can occur when the period (the separation of the periodic dielectric materials) is less than the wavelength of the light. If the choice of lattice geometries and compositional dielectric materials are suitable, it is possible all those reflection and refractions will cancel not only the light scattered sideways, but the light moving forward as well. Then, because the light has to go somewhere (energy is conversed), it has no choice but to go back, which in this case it is forbidden from entering the photonic crystals. This happens no matter what direction the light is coming from, in a certain range of wavelengths which called *photonic band gap*.

Fundamentally, PhCs are based on a concept of extended from conventional diffraction gratings and have unique analogy to solid state crystals. Thus the solid state physics theory is used for the analysis of PhCs. For example, one can calculate photonic band gaps (PBGs), impurity, defects and surface states, for PhCs structure. This allows the manipulation of light in dielectric mediums. For example, by carving a tunnel through the material, an optical "wire" can be created which no light can be deviate in the "wire". Also, by making a cavity in the center of the crystals, the beam of light could be caught and held which created an optical "cage". The abilities to trap and guide light have many potential applications in optical communications and computing, where one would like to make tiny optical "circuits" to help manage the ever-increasing traffic through the world's optical communications networks. Other devices, too, are made possible by this increased control over light: from more-efficient lasers and LED light sources, to opening new regimes for operating optical fibers, to cellular phones.

2. Application and fabrication of photonic crystals devices

2.1 The application of photonic crystals

Photonic crystals are attractive optical materials for controlling and manipulating the flow of light. One dimensional photonic crystals are already in widespread use in the form of thin-film optics with applications ranging from low and high reflection coatings on lenses and mirrors to colour changing paints and inks. Higher dimensional photonic crystals are of great interest for both fundamental and applied research, and the two dimensional ones are

beginning to find commercial applications. K. Inoue have summarizes the relation of PhCs with other optics and various applications now being developed as shown in Fig.1. Considering that PhCs exhibit their functionalities by multidiffraction and multiscattering, a PhC can be said to be a kind of hologram in a broad sense. A novelty of PhCs, compared with conventional holograms, is the precise design method, namely the photonic band calculation, which is very effective for estimating their functionalities and performance.
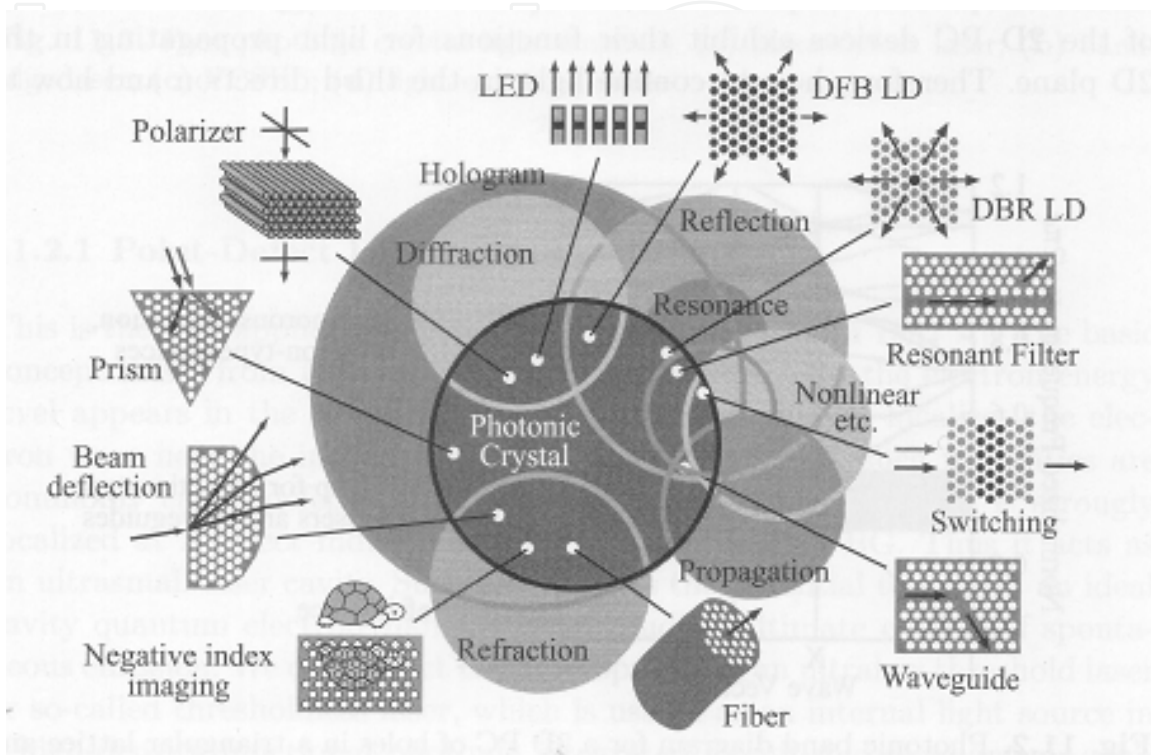

Fig. 1. Photonic crystal optics and various applications (Source: K. Inoue et al. 2004)

Many applications of two dimensional photonic crystals are directed towards integration of photonic devices. It is important to evolve into the photonic and electronics circuits, which will require high-density photonic and electronic circuits. The example of photonic crystals devices is LED, waveguide, resonator and photonic crystal fiber.

The introduction of defects into photonic lattices results in generation of a defect level and light is confined to be localized defect state. This high quality factor selection of one wavelength within the band gap can be used to make devices which combine advantages of thresholdless light emission and high reliability of LEDs with coherence and high efficiency of lasers. PhCs have also been used just as confining regions for lasers. Lasers have been fabricated with a 2D photonic lattice as mirrors instead of cleaved facets.

Artificial defects in PhCs and related formation on defect state within the band gap has been used in the realization of the devices such as filters and resonators. The confinement properties along with the defect properties can be used in various other applications such as sharp waveguide bends, fabry-perot cavity and reflection type lens.

Waveguiding of light within a photonic lattice with a defect region guiding light has been widely reported with near perfect transmission. The property is can be particularly useful for applications which need data transmission through bends whose feature size are in the nano meter rangers.

PhC also have been used as a clad of optical fibers for better confinement. One type of such a fiber uses the low effective refractive index of the PhC for optical confinement. Other such fibers use bragg reflection of PhCs or bragg reflection of a coaxial multilayer mirror. All such fiber predominantly use an air core and single mode PBG guidance has been demonstrated.

Anomalous dispersion and anistropic properties of PhCs have been used to fabricate optical components like prisms and polarizers. Wavelength dependent angular dispersion of PhCs is about hundred times more than in an ordinary prism. This phenomenon is termed as superprism phenomenon and is expected to be very useful in applications such as wavelength division multiplexing. A Si/SiO_2 multilayer with a zigzag cross section was fabricated and was found to work

The photonic band diagram indicates that there are three different frequency ranges for light, which can be utilized for real applications, as shown in Fig 2. The first one is the lowest frequency range below the first zone folding of the photonic band. The gradient of the lowest straight photonic band is determined by the effective refractive index n of the PhC and it is different for different polarizations. Classically, this characterization is called form birefringence. Since the PBG calculation precisely predicts the effective index for each polarization, the index is artificially controlled by the PhC structure. The second one is photonic band gap, which means the omni-directional stop band. It is one of the most unique properties of PhCs, and actually it was the main topic at the early stage of PhC research.

The photonic band gap can be used as a reflector for light that is to enter the PhC from arbitrary directions. It is applied to reflection-type devices, e.g., lasers and waveguides. The third one is the higher frequency range above the photonic band gap where complex photonic bands exist. The slope of a photonic band is proportional to the group velocity of the light. Therefore, the horizontal band at a band-edge means zero vg and the localization of light energy. In 2D and 3D PhCs, such a zero velocity group or a small velocity group appears not only at the band-edge but in many bands. They will be effective for the enhancement of various interactions of light with materials of the PhC. In addition, the 2D or 3D distribution of bands, the so called dispersion surface, provides unique light propagation in PhCs. Thus, this frequency range can be used in transmission-type functional devices.
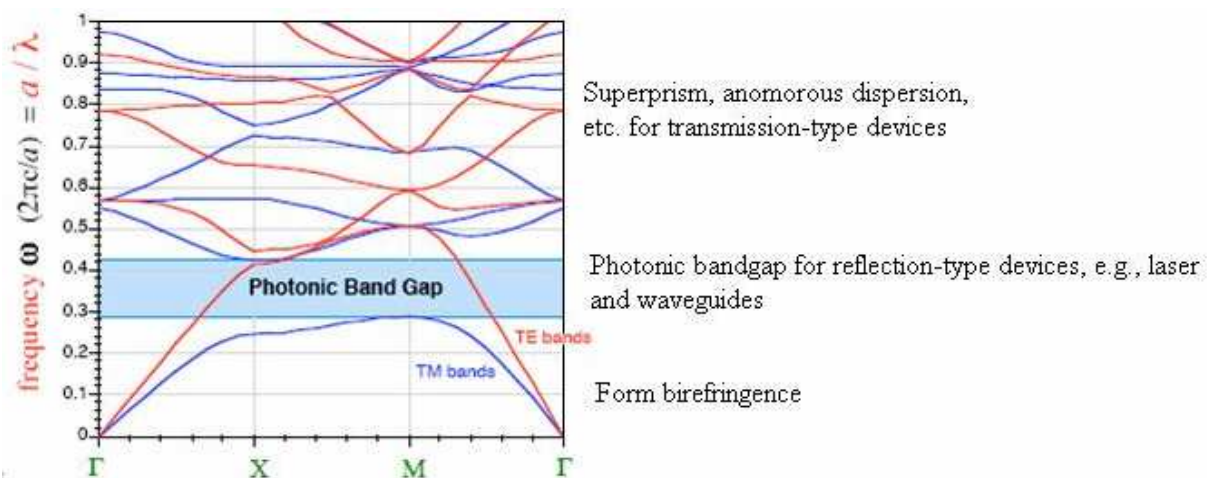

Fig. 2. Photonic band diagram for 2D PhC of holes in a triangular lattice and three frequency ranges for different application targets. (Source: K. Inoue et al. 2004)

2.2 Fabrication of photonic crystals waveguide

Fabrication of two dimensional photonic structures requires one to mark the planar pattern of unwanted areas on the surface of the semiconductor, and remove the material from these areas, thus creating holes and it is vice versa for creating pillars. Dry etching by reactive ions or wet electrochemical etching are most often employed for this purpose. Dry etching allows accurate control over the hole size and arrangement (with nanometer precision), but has limited maximum depth of etching. It is therefore used to fabricate low aspect ratio structures, such as thin waveguides. Electrochemical etching allows one to obtain very deep holes, and is suitable for fabricating high aspect ratio structures, but the size of etched holes can be controlled somewhat less predictably.

Marking of the unwanted areas is usually done by lithography. Since the most promising structures are those having photonic band gaps near-infrared and visible ranges, they must have features of comparable size, and conventional lithography cannot be applied. Thus, electron beam lithography (EBL) is used, which normally employs a scanning electron microscope with resolution around 1 nm, equipped with an electron beam drawing stage to transfer preset patterns on the surface of a semiconductor wafer, covered by photoresists, e.g. a layer of PMMA with 200-400 nm thickness. The pattern resulting after the photoresist development is used as a mask for subsequent etching.

The etching is done by reactive ions, accelerated towards the sample surface in a plasma discharge, and reacting with the material in the unmasked areas, thus destroying it. Typically, chlorine-based ($SiCl_4$ and Cl_2), or fluorine-based (CHF_3, CF_4, C_2F_6 and SF_6) reactive gases are used. For etching GaAs and AlGaAs structures, use of clorine-based gases has become standard, while fluorine-based etching chemistry is preferred for silicon. Reactive ion etching is highly anistropic, and therefore the initial mask pattern does not spread out laterally with increasing etching depth, and deep holes with almost parallel walls are obtained. The etching also destroys photoresists, albeit it is slower rate, which depends on the details of the etching process and photoresists parameters. Since etching must be stopped before mask becomes unrealiable, this factor limits the maximum achievable aspect ratio to about 10. To increase the aspect ratio, masks highly resistant to reactive etching (typically Au, Cr, SiO2 or Si_3N_4) are deposited and patterned on the surface using lithography, and etching is carried out with fluorine gases. As a result, photonic crystal structures with aspect ratios up to 20 were successfully fabricated.

3. Photonic band gap in 2-D photonic crystals

One of the most important features in photonic crystals is the photonic band gap (PBG), which is analogous to band gaps or energy gaps for electrons travelling in semiconductors. In the case of semiconductors, a band gap arises from the wave-like natures of electrons. Electrons as waves within a semiconductor experience periodic potential from each atom and are reflected by the atoms. Under certain conditions, electrons with certain wave vectors and energy constitute standing waves. The range of energy, named "band gap" in which electrons are not allowed to exist, appears. This phenomenon differentiates semiconductors from metal and insulators. In the similar manner, standing waves of electromagnetic waves can propagate through a periodic structure whose minimum features are less than the wavelength of light. In this case, the medium expels photons with certain wavelengths and wave vectors. Such a structure acts as an insulator of light, and this phenomenon is referred to as "photonic band gap".
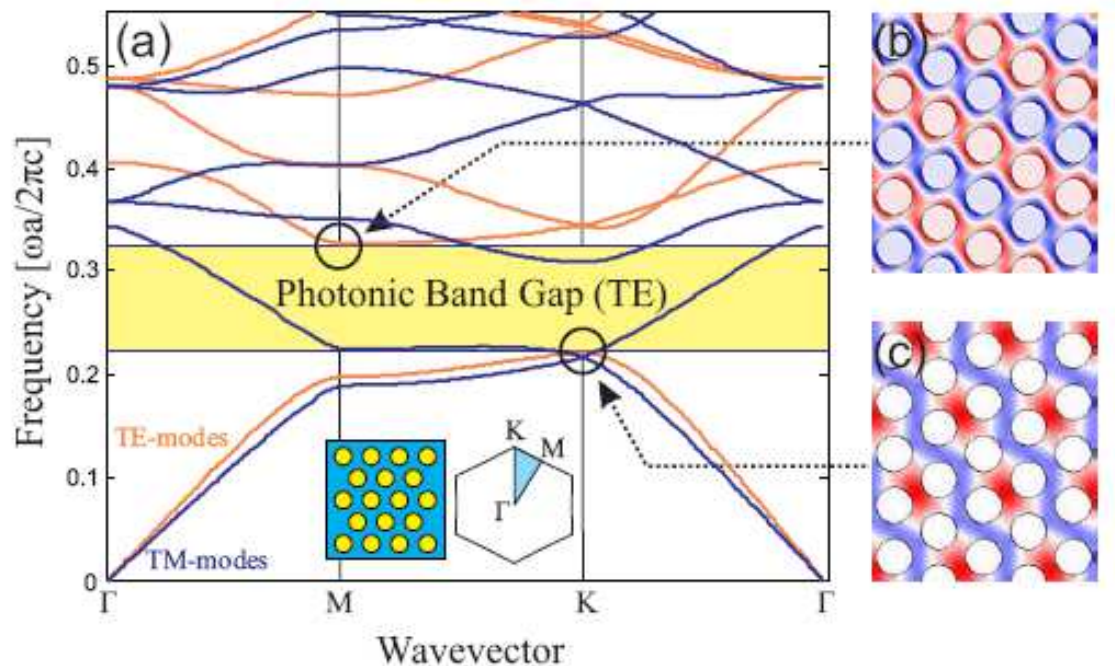
Fig. 3. (*a*) The photonic band structure for a triangular lattice of holes in a high index material. The frequencies for the two polarizations (TE modes in light gray, TM modes in dark gray) are plotted around the boundary of the irreducible Brillouin zone (shaded triangle in the inset). (*b*) The magnet field pattern of the TE mode corresponding to the second band at the first M point. (*c*) The magnetic field pattern of the TE mode corresponding to the first band at the K point. The grey levels indicated the amplitude of the magnetic field (dark-negative, light-positive). There is a band for the TE guided modes only.

A first characteristic optical property of PhC is the PBG. A two-dimensional triangular lattice with a hexagonal Brillouin zone exhibits a very high symmetry in the plane. Therefore, this structure is convenient for the formation of forbidden bands in all directions with the plane of periodicity. Fig. 3 shows the photonic band structure or dispersion diagram with the eigensolutions for a triangular lattice of holes in a high refractive index material. Both TE and the TM band structures are shown. The in-plane wavevector $\mathbf{k}_{//}$ goes along the edge of irreducible Brillouin zone, from Γ to M to K as shown in the inset in Fig. 3 (a). It is conventional to plot the frequency bands only extrema almost always occur along these boundaries. For TE modes (light gray lines in Fig.3 (a), there is no photonic band gap exists.

In order to understand in more detail the formation of photonic band gap for TE modes, the field patterns (magnetic field) at the lower and upper band edges corresponding to the high symmetry points K and M of the irreducible Brillouin zone was analyzed. At the lower band edge, the field associated with the lowest TE mode at K is strongly concerted in the high index material (Fig. 3 (a)) giving it a lower frequency. In contrast, the field pattern of the second mode at M, the upper band edge, has a nodal plane cutting through the high index material and therefore its energy is more concentrated in the air holes (Fig. 3(b)) giving it a higher frequency. For this reason, the bands above and below PBG are also referred to "air band" and "dielectric band", respectively. The PBG arises from this difference in field energy distribution. The higher the dielectric contrast in the periodic structure the larger is the PBG. Therefore, high index materials are essential for the realization of PhC structures.

Fig. 4 shows example of gap map plot for square, hexagon and circular scatterers pillars in honeycomb lattice. A gap map is a plot of the locations of the photonic band gaps of a crystal, as one or more of the parameters of the crystal are varied. The red and blue gaps show the TE band gap and TM band gap, respectively. Meanwhile, the green gaps show the absolute band gap which the TE and TM band gap overlap. As can be seen all three structures in honeycomb lattice have absolute band gap and the gaps all decrease in frequency as the filling fraction increases.
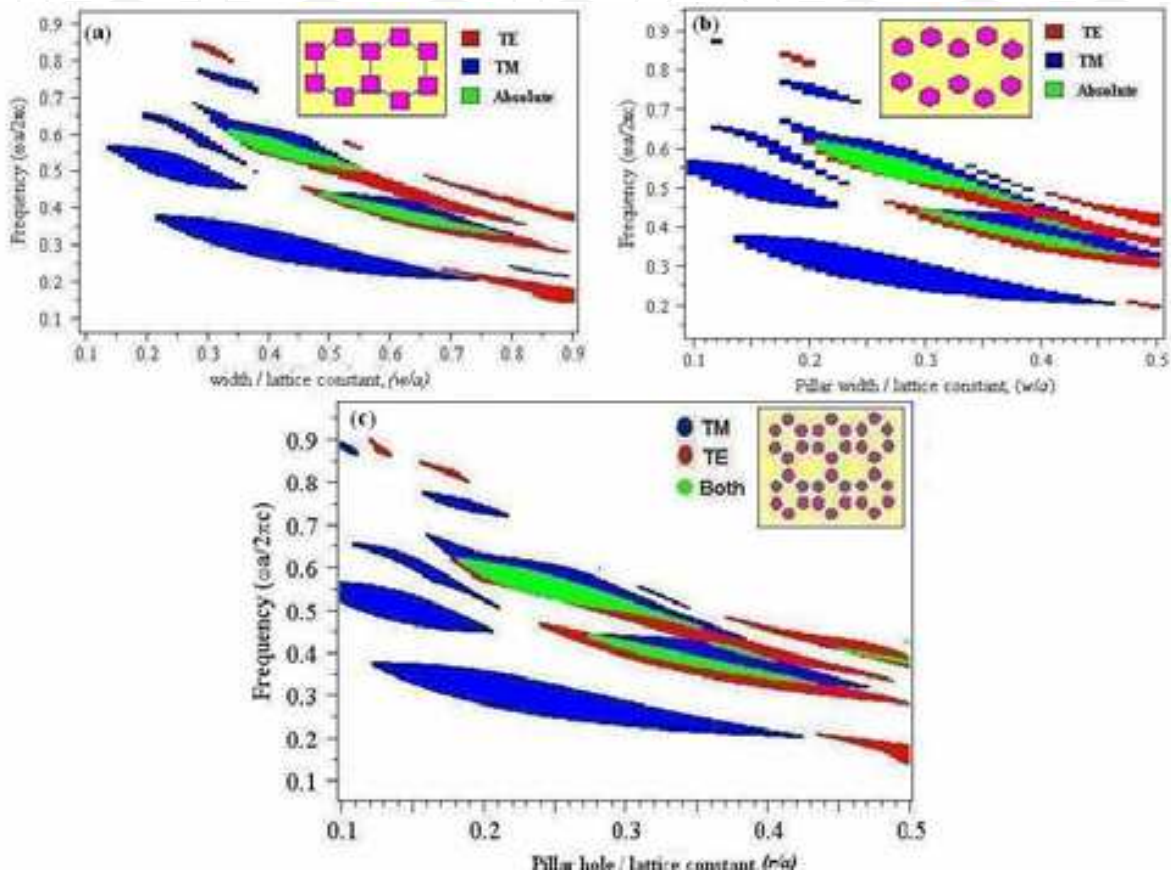
Fig. 4. Gap map for (a) Square scatterer pillars, (b) Hexagon scatterer pillar and (c) circular scatterer pillar in honey comb lattice

4. Defect engineering in photonic crystals waveguide

In the same way as for solid-state crystals, two main types of defects exist: cavities defects and extended defects. Cavities defects are associated to very local disruptions in the periodicity of the crystal, and their presence is revealed through the appearance of electromagnetic modes at discrete frequencies, which may be seen as analogous to isolated electronic states. Likewise, extended defects can be seen as analogous to dislocations of the crystal, and they may result in the appearance of transmission bands in spectral regions where a photonic band gap existed in the case of a perfectly periodic crystal.

Fig. 5 show the schematic illustration of possible defects in PhC. A single pillar from the crystal can be remove, or replace it with another whose size, shape, or dielectric constant is different than the original. Cavities and extended defects can be used to create a basic waveguiding component such as waveguide and bend waveguide.
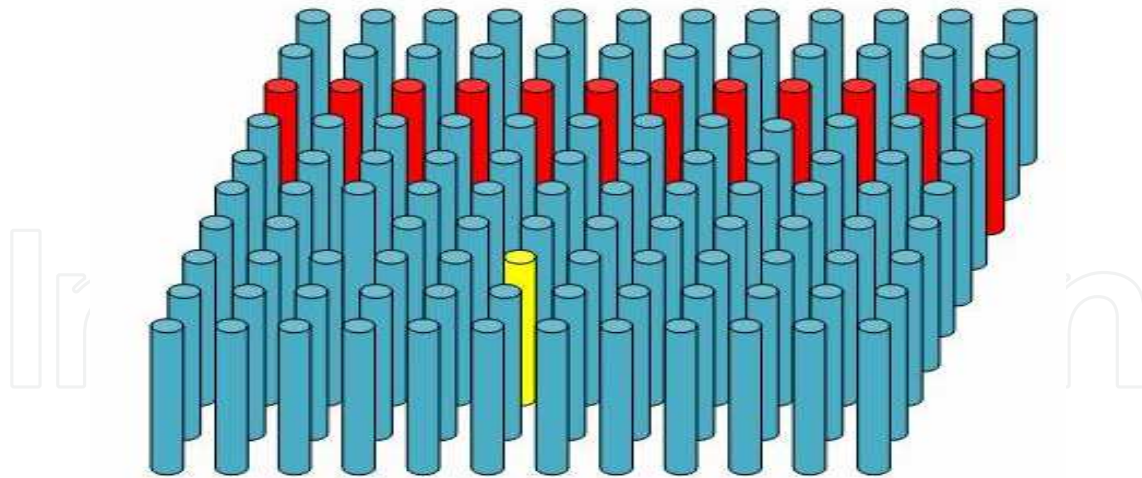
Fig. 5. Schematic illustrations of possible defects in PhC. Perturbing the line of pillar (red) might allow a localized state to exist. Perturbing one pillar in the bulk of the crystal (yellow) might allow a localized defect state to exist.

4.1 Cavities defects

Cavities defects can be created by locally modifying the refractive index, by changing the size of the patterns (substitution defect), by displacing one of the periodic patterns (interstitial defect) or by inserting a different pattern (dopant). Here again, the presence of a point defect may lead to discrete energy levels within the photonic gaps. Point defects in two-dimensional photonic crystals, correspond to localized electromagnetic modes in the case where the band gaps are omnidirectional, be it only for certain polarization. If this condition fulfilled, the electromagnetic field is actually found to be concentrated in the region of the defect and evanescent in the surrounding regions. By contrast, in the case where the band gap is not omnidirectional, a fraction of the electromagnetic energy will constantly leak away from the region of the defect towards directions along which the propagation is allowed. In this case, the presence of a point defect essentially leads to a peak in the density of electromagnetics states.

By removing a pillar from the lattice, we create a cavity that is effectively surrounded by reflecting walls. If the cavity has the proper size to support a mode in the band gap, then light cannot escape and we can pin the mode to the defect. In fact, a resonant cavity would be useful whenever one would like to control radiation within a narrow frequency range.

The important questions to address when designing a defect mode are how the defect shall be introduced into the structure, and which frequencies it will support as localized modes. First, one obvious way to introduce defect is allow one of the pillars of the rectangular lattice to grow or shrink in radius, calling the radius of the defect pillar is r_{def}, the possibilities range from $r_{def} = 0$, corresponding to missing pillar in the structure, to around $r_{def} = 0.5a$ μm, corresponding to an pillar that envelops one entire unit cell.

Next, we would like the defect to harbor modes of light that have frequencies within the band gap of the crystal. Fig. 6 shows the defect frequencies as the defect radius varies across the entire range in silicon rectangular pillars. The defect pillar is surrounded by perfect lattice at $r = 0.18a$. The photonic band gap is a white space between upper and lower green block which around frequency 0.30 to 0.445. From the plot, it shows that the bigger the defect pillar, the great quantity of defect modes occurred.
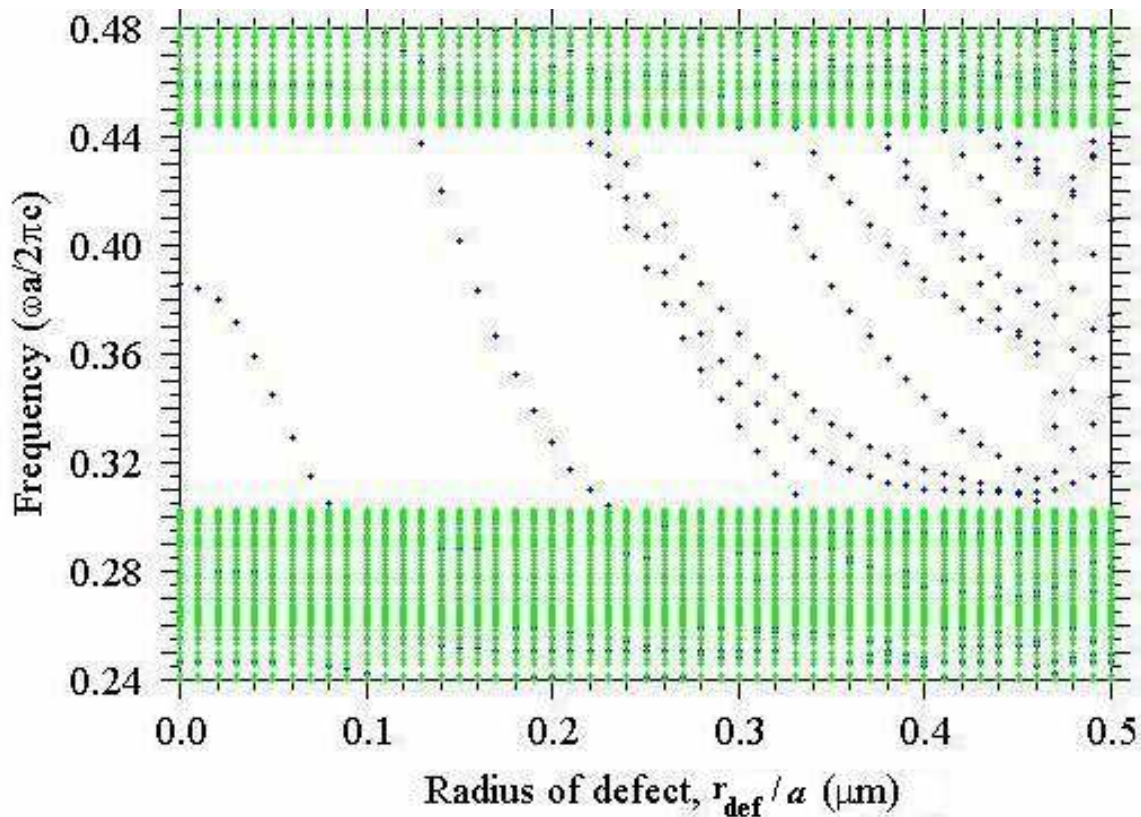
Fig. 6. A plot of the TM modes in rectangular silicon pillars in air with *r*= 0.18*a*. The photonic band gap is the white space between green block. The localized modes are shown as blue dotted lines. We create the defect cavity filling in a single silicon pillar.

Note that it is possible not only to create a defect mode with a frequency in the band gap, but also that the defect frequency sweeps continuously across the band gap as r_{def} is varied. In other words, we can "tune" the defect frequency or later called resonant frequency to any value within the band gap with a judicious choice of r_{def}. This complete tenability is an important feature of PhCs, it would be analogous to the ability to tune the properties of solids by somehow adjusting the radii of single dopant atoms.

Fig. 7 show the defect characteristics when a single missing pillar is involved at the centered of perfect circular pillar-type in rectangular lattice of PhC. Fig. 7 (a) represents the field distributions calculated for a defect created in a two-dimensional square lattice formed by dielectric pillars in air. The defect was created here by removing one pillar. The incident wave is assumed to be TM polarized. Removing one pillar introduce a peak into the crystal's density of states. In fig. 7 (b), the peak happens to be located in the photonic band gap which located in the yellow gap, then the defect-induced state must be evanescent-the defect mode cannot penetrate to the rest of the crystal, since it has frequency in the band gap. In this case a single missing pillar emits the resonant wavelength of 1.47 µm.

When several point defects of the same nature are present in a photonic crystal, and when the distance between these defects is large enough, their mutual influence can be neglected. In this case, everything happens as if an energy degeneracy of the system occurred several times. Indeed, while the electromagnetic modes associated to the different defects are localized in different region of the crystal, their field distributions are identical. By contrast, when the distance between the defects decreases, the coupling between these defects leads
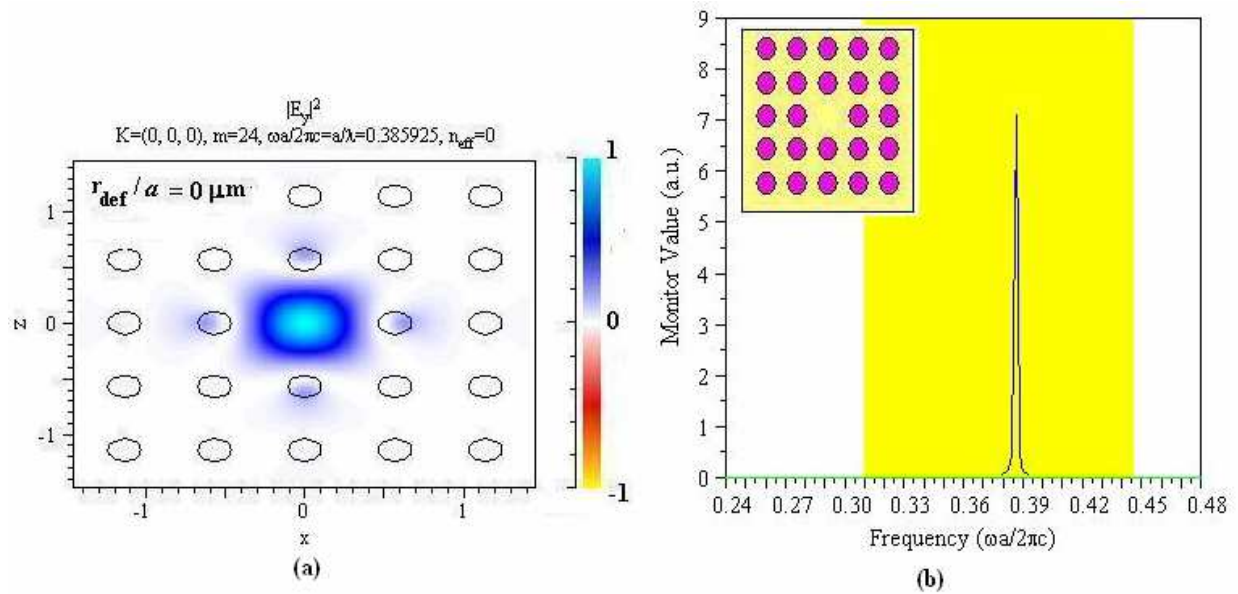
Fig. 7. Defect in a rectangular missing single pillar (*rdef* = 0). (a) The electric field patterns of the defect modes with defect frequency of 0.386. The panel at the most right side of (a) indicate the strength of the field. (b) The resonant frequency spectrum found from impulse simulation of the defect structure. The peak at 0.387 $\omega a/2\pi c$ represents a wavelength of 1.47µm.

to the formation of electromagnetic modes with different field distributions: in this case, the energy degeneracy is lifted. Fig.8 illustrates the effects induced by such a coupling through spectral measurement performed using FDTD. Two were introduced by removing two dielectric pillars. The transmission spectrum of the crystal was then measured for two different distances between the defects.
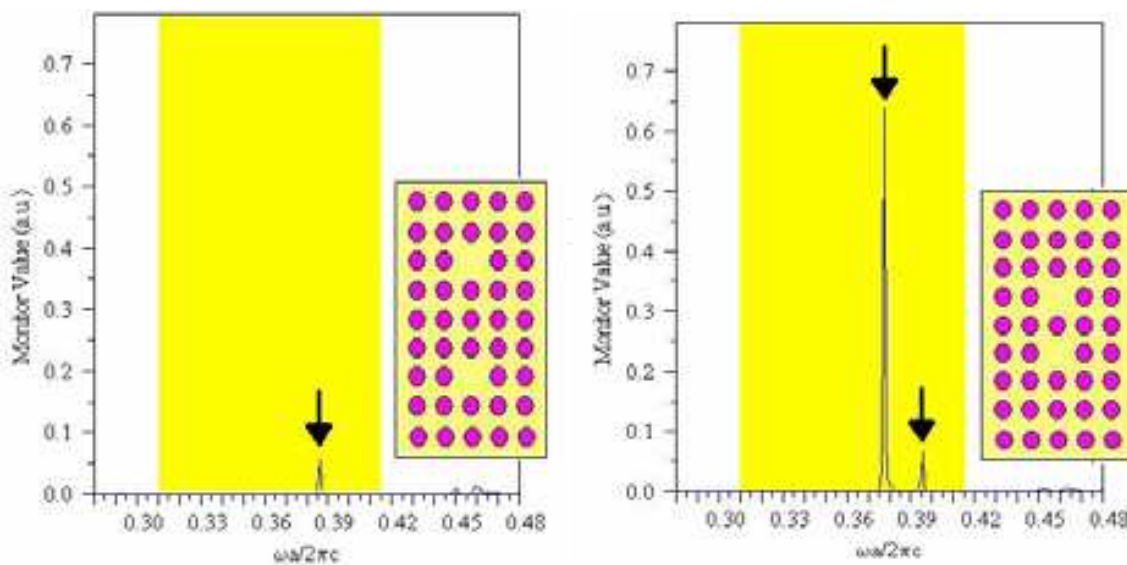
Fig. 8. Coupling between two point defects in a two-dimensional photonic crystal with a square symmetry. The crystal here is formed by a lattice of silicon pillars extending in the air. *Left*. Transmission spectrum measured in weak coupling regime. *Right*. Transmission spectrum measured in strong coupling regime.

When the two defects are distant from one another, as in the case in the left part of Fig. 8, a single transmission peak is observed at the high-frequency side of the TE band gap. This corresponds to an air defect, according to the terminology used in (Joannopolous, 1995). When the defects are at close distant from one another, the transmission maximum splits into two peaks, thereby revealing the existence of two different electromagnetic modes. Assuming the origin to be at the centre of the structure, the low-frequency mode presents a symmetric field distribution, while the high-frequency mode presents an anti-symmetric field distribution. This phenomenon is quite analogous to the situation occurring when a particle is released in a quantum well (Cohen-Tannoudji, 1973): the wave function of the fundamental state is symmetric whereas the wave function of the first excited state is anti-symmetric.

4.2 Extended defects

We can use cavities defects in photonic crystals to trap light, as we have seen in point defect. By using extended defects or line defects, we can also guide light from one location to another. The basic idea is to carve a waveguide out of an otherwise-perfect photonic crystal. Light that propagates in the waveguide with a frequency within the band gap of the crystal is confined to, and can be directed along the waveguide.

In Fig.9 (a) we show the band structure for the guide created by removing a row of pillars in the direction of the crystal, as shown in the inset. We find a single guided mode inside the band gap. The electric field of the mode has even symmetry with respect to the mirror plane along the guide axis. The mode itself bears a close resemblance to the fundamental mode of a conventional dielectric waveguide: it has sinusoidal profile inside the guide and decays exponentially outside.

In Fig.9 (b) the waveguide is made by removing three rows of pillars in the direction of the crystal (see the inset). There are now three guided modes inside the gap that can again be classified according to their symmetry with respect to the mirror plane along guide axis. The first and the second modes are even, whereas the third mode is odd.

It is generally true that the number of bands inside the band gap equals the number of rows of pillars removed when creating the guide. This can be understood from a simple counting of states in the crystal. If we decrease the dielectric constant of a single pillar in a prefect crystal, we pull up one defect state from the dielectric band. If we repeat this for a whole row of pillars, we pull up N localized states in an N x N crystal: one state at each k point for **k** along the guide. Analogously, when M rows of pillars are removed, we pull up M guided modes at each **k** from the dielectric band. Nevertheless, at some **k**'s the modes may have frequencies outside the band gap and the entire band may not be contained in the gap, as is the case, for instance for the lowest guided mode band in Fig.9 (b).

Next we want to see what happen if we removed single row of pillar and then we put defect along the waveguide as shown in Fig.10 (a) which also known as couple cavity waveguide.

Fig. 10 (b) shows the transmission spectra of couple cavity waveguide over the wavelength as the radius of the cavity defect is varied. The radius is varied from $0.1a$ to $0.4a$. Obviously from the graph we can see that this structure can be made as filter. For example if we want to filter wavelength 1.31 μm and 1.55 μm separately, we can include radius defect of $0.3a$ along the waveguide to block wavelength 1.31 μm from entering the waveguide and wavelength 1.55μm is allow to enter the waveguide. The wavelength of 1.55 μm can be

block from entering the waveguide by include the radius defect $0.2a$. It can be noticed that when defect radius increases, the guided frequencies shift towards higher wavelengths. As the defect increases, the miniband is nearer to the dielectric band and also the modes can interact with in the bulk modes and, as a result of that, the transmission loss increases slightly.
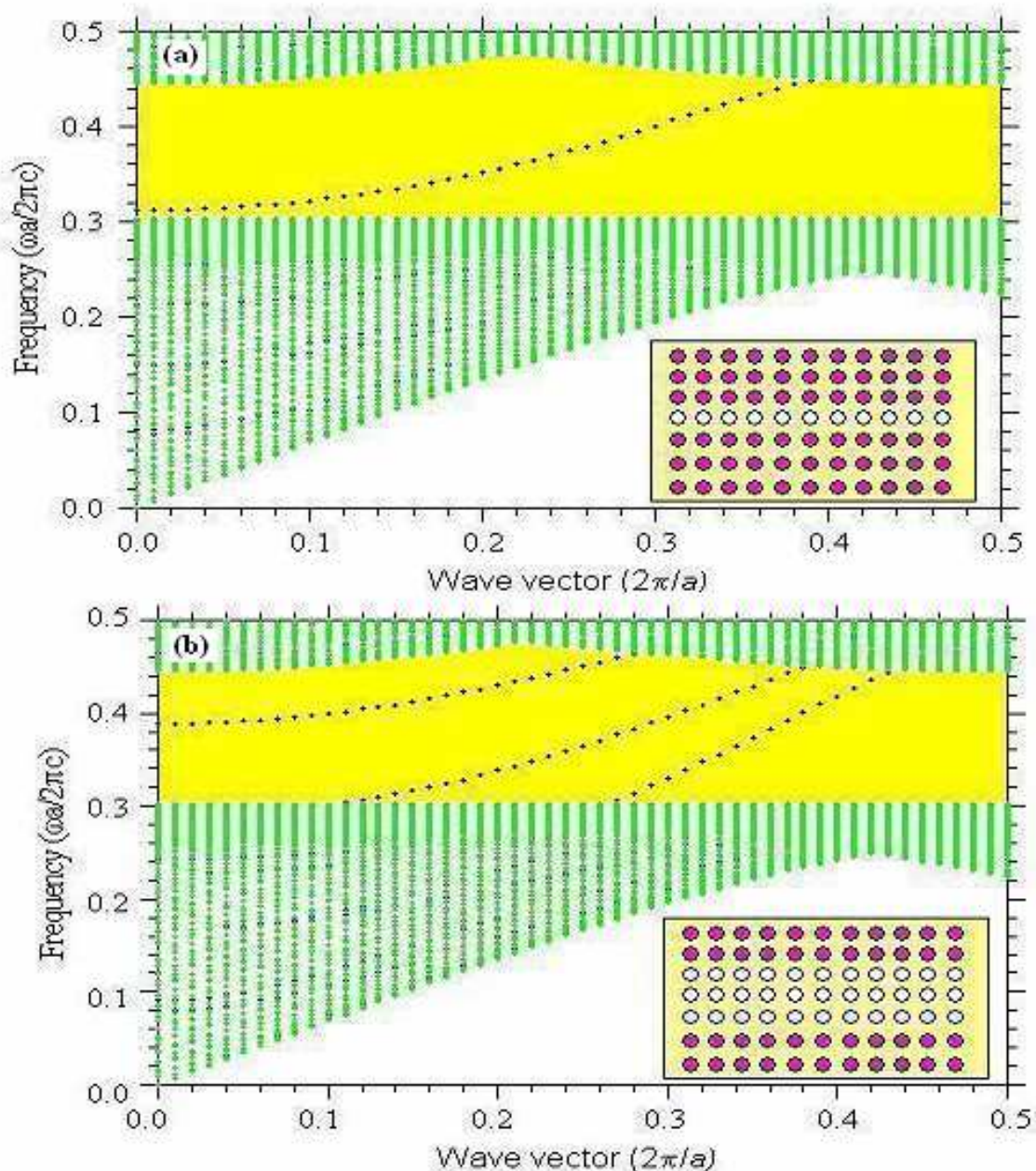

Fig 9. The projected band structure of TM modes for a waveguide in a square lattice of silicon pillars in air. The green region contains continuum of extended crystal states. The photonic band gap is colored yellow. The black dotted point is the band of guided modes that runs along the waveguide. (a) The waveguide is formed by removing one row of silicon pillar as shown in the inset. (b) . The waveguide is formed by removing three row of silicon pillar as shown in the inset.
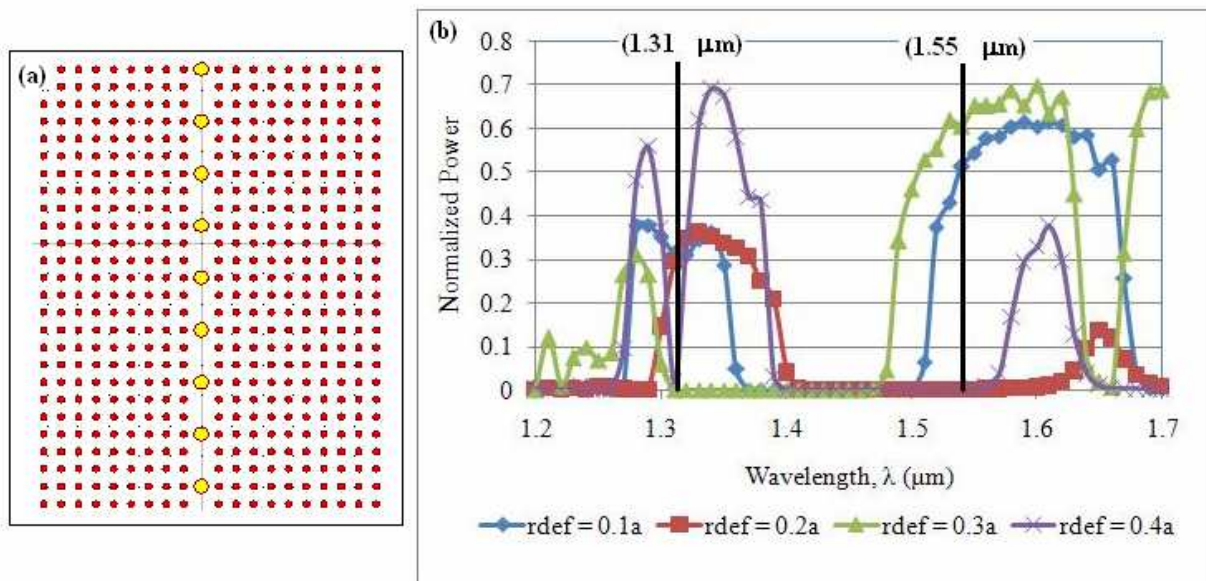
Fig. 10. (a) Couple cavity waveguide. (b) Transmission spectra of couple cavity waveguide as radius of the cavity are varied.

Fig.11 shows the projected band structured and dispersion curve for (a) coupling of two waveguide and (b) coupling of three waveguides. The PhC bands are shaded green and the bandgap is the gap between the two shaded green. In contrast to the waveguide modes in single missing row as shown in Fig.11 (a), there is at most one guided mode for all frequencies in the band gap. This is a property of common to most single line defect waveguides. In Fig.11 (a) there are two guided modes for coupling of two waveguide structure. At the small wavevector the guided modes is not couple together but as the wavevector increase, the two modes seem to couple together. The figure at the right inset of Fig.11 (a) show the enlarge point at the wavevector of 0.37 to 0.41. we can seen clearly that the two guided modes separate at wavevector 0.37, couple at point 0.385 and decouple back at point 0.39.

Fig.11 (b) shows the characteristics of guided modes for coupling of three waveguides. The right inside of Fig.11 (b) shows the two guide modes not couple to each other along the wavevector. A conclusion can be made, when two parallel identical PhC waveguides are brought close enough to have defect modes well coupled, the defect modes will split into two eigenmodes. The smaller the separation of waveguides, the larger the coupling and the more splitting in dispersion of the eigenmodes.

In this next section we want to show that photonic crystal can be use to guide light around the tight corners. In rectangular lattice, we can carve out a waveguide with a sharp 90 degree bend as shown in Fig. 12. Here we plot the displacement field of propagating TM mode as it travels around the corner. Even though the radius of the curvature of the bend is less than the wavelength of the light, very nearly all the light that goes in one end comes out the other.

Fig. 13 shows the loss over wavelength for 90°. The transmission loss for 90° bend along the telecommunication regime can be achieved less than 5 dB. The reflectivity at this sharp corner is around 0-15 dB. This figure proved that the PhC is a suitable material to guide light in very sharp corner with very small loss compare to conventional waveguide which loss usually 13-40 dB.
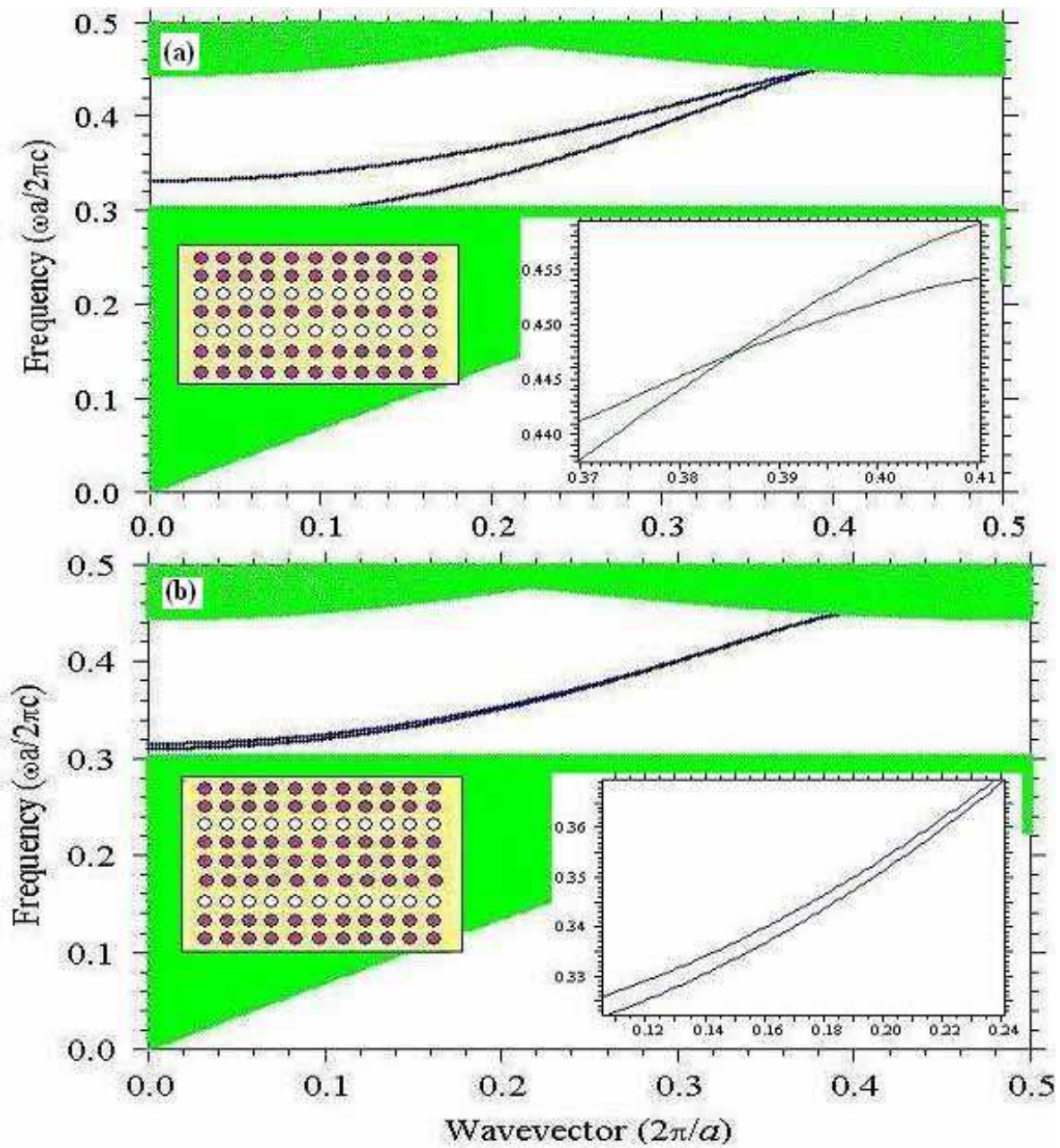
Fig. 11. Geometries and band structures for one (a) and three rows of dielectric pillars between two parallel waveguides. Enlarged parts of the band structures are shown in the insets of (a) and (b) to illustrate that the bands cross in (a) but do not cross in (b).
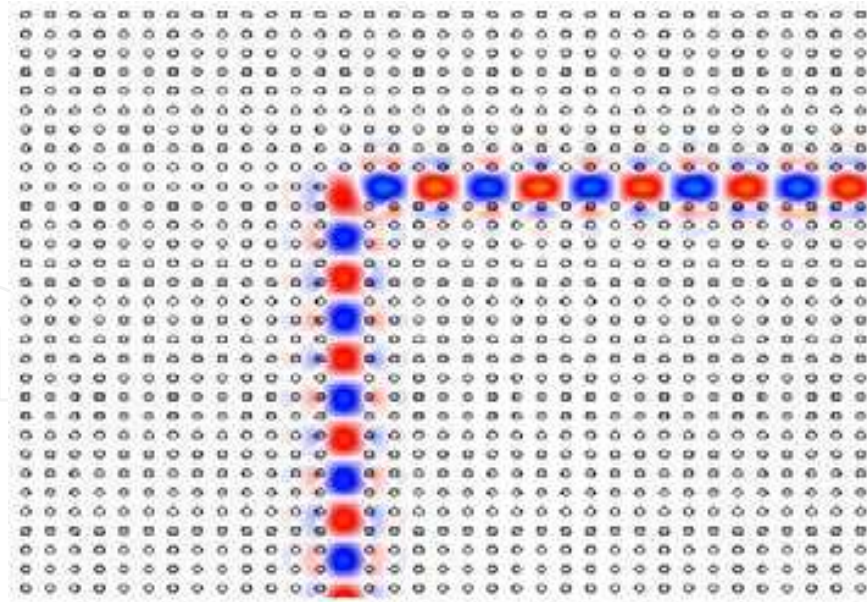
Fig. 12. The displacement field of a TM mode traveling around a sharp bend in a waveguide carved out of a rectangular lattice of dielectric pillars. Light is coming in from the bottom and exiting at the right.
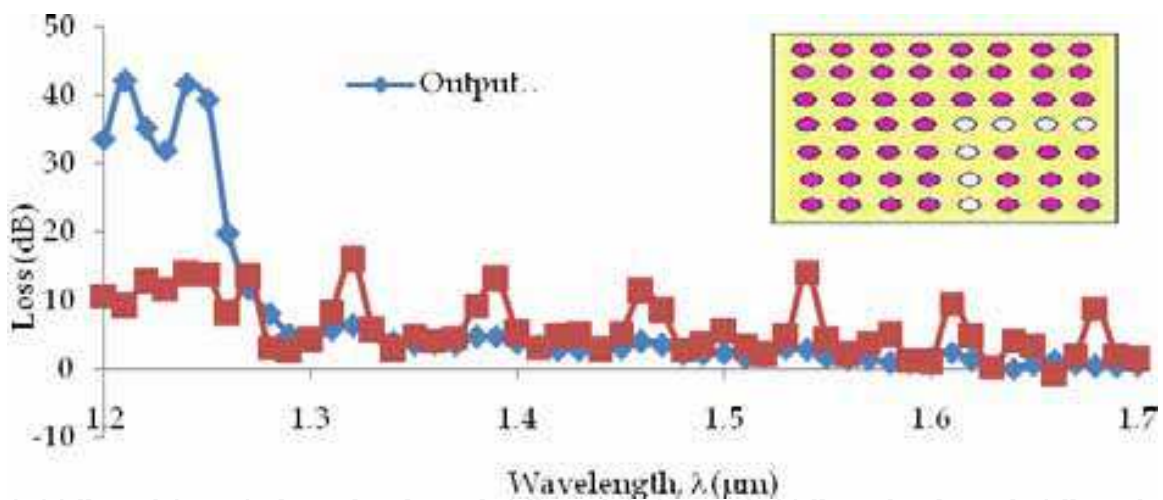

Fig. 13. Loss over wavelength for 90° bend.

5. Photonic crystals multiplexer/demultiplexer devices

A PhC with photonic band gap is a promising candidate as a platform on which to construct devices with dimensions of several wavelengths for future photonic integrated circuits. PhCs are particularly interesting, in all-optical systems to transmission and processing information due to the effect of localization of the light in the defect region of the periodic structure. Among the most important application areas of PhCs is low threshold single mode lasers (where PhCs are used as the optical confinement factor), wavelength filters, optical waveguide structures, WDM system devices, splitters and combiners. Wavelength filters of optical range based of two dimensional PBG structure can be created by the correct selection of geometrical and physical parameters.

In this subchapter, two wavelength demultiplexer/multiplexers (DEMUX/MUX) are designed. These DEMUX/MUXs consist of circular pillars in rectangular lattice surrounded by air with radius of circular scatterers is 0.18a. Device A which is 1310 nm / 1550 nm DEMUX/MUX device is based on splitting the wavelength channel using wide band filters. Finally, device B which split 1310 nm and 1550 nm wavelength channels was using MMI splitting mechanism.

5.1 Device A: 1310 nm /1550 nm Demultiplexer/Multiplexer

Fig. 14. shows the schematic diagram of 1310/1550 nm demultiplexer for rectangular lattice of silicon pillars. Two filters with radius defect inside it is placed at the T-junction. Filter 1 has radius defect of r_1 = 0.11a which only filter wavelength 1310 nm and filter 2 has radius defect of r_2 = 0.25a and absolutely only emit wavelength 1310 nm inside it.
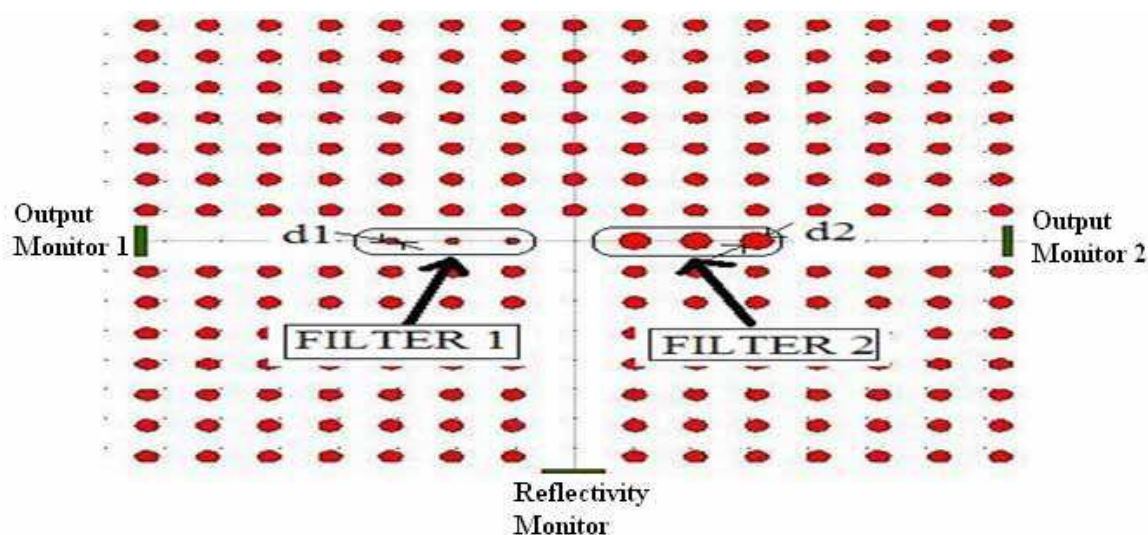

Fig. 14. Schematic diagram of the optical DEMUX/MUX based on a PhC waveguide with filter 1 and filter 2

The characteristics of defect pillars in filter 1 and filter 2 is investigated. The effect of number of pillar towards transmission power and reflectivity inside the filter was studied intensively. The output monitor of filter 1 is placed at left side of filter 1, meanwhile output monitor of filter 2 is placed at the right most of the waveguide and finally monitor for reflectivity is placed at the back of input signal as shown in fig. 14.

Fig. 15 shows the transmission characteristics at filter 1, filter 2 and reflectivity at varies number of defect pillars at input wavelength of 1310 nm. Basically when the wavelength of 1310 nm propagates inside the device A, it penetrate the filter 1. At filter 2, the maximum of 40% power is detected at monitor 2 and maximum power of 38% was reflect back at reflectivity monitor.

Fig. 15 (b) shows the normalized power inside the filter 2. Power occurred inside this filter is called crosstalk. For ideal case, power should be zero at this monitor 2 meanwhile power should transmit 100% at monitor 1. Unfortunately it did not happen in our device A because small amount of power dissipate into filter 2 and reflect back. The minimum number of defect pillars inside the filter caused the maximum crosstalk inside the device A.
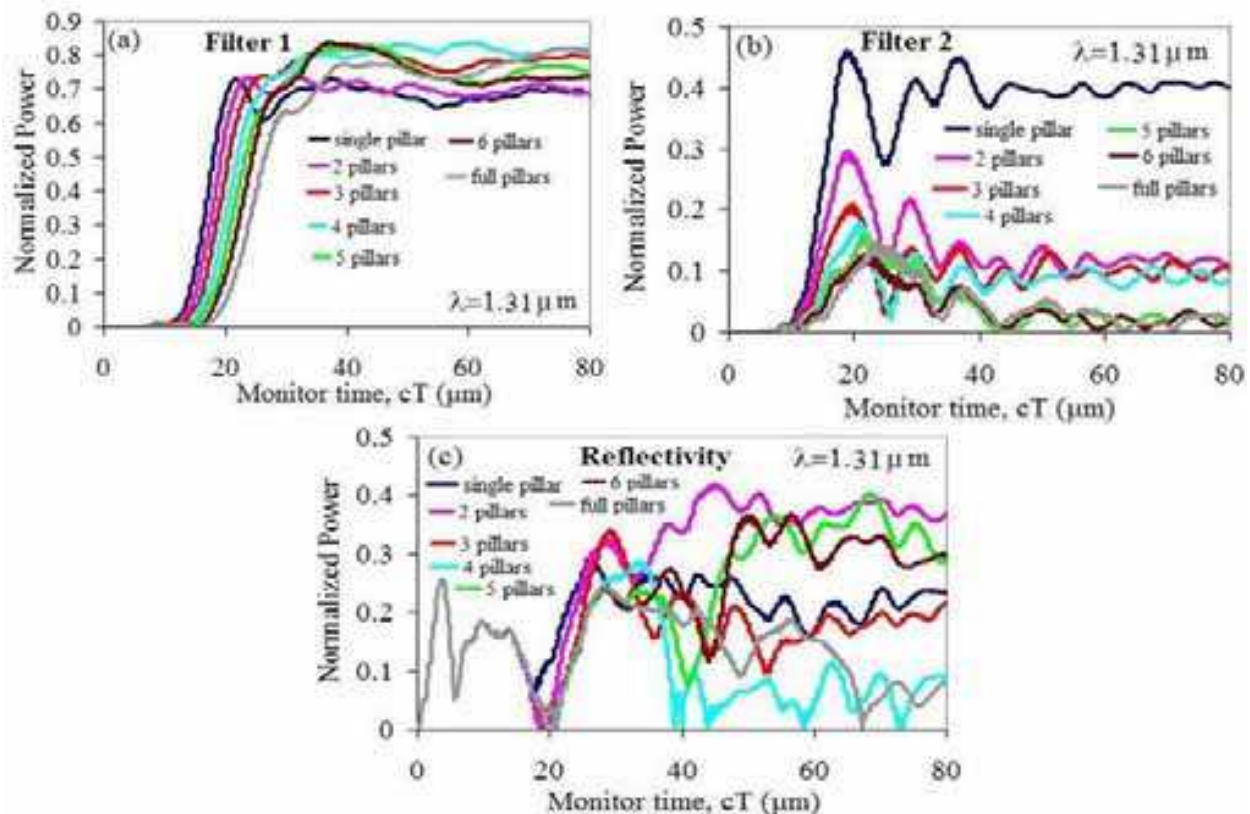
Fig. 15. Transmission characteristics inside filter 1, filter 2 and reflectivity when wavelength, λ of 1310 nm propagate inside device A.

A small amount of power was reflected back when all the pillars is occupied inside both filters as shown in fig.15 (c). Average of 24% power is reflected back when the wavelength of 1310 nm propagate inside device A.

Fig. 16 shows transmission characteristics at monitor 1, monitor 2 and reflectivity monitor when wavelength 1550 nm propagates inside device A. As can been seen, the filter at each arms work correctly because the power detected at monitor 1 is minimum meanwhile the power is maximum at monitor 2. This situation is vice versa when wavelength of 1310 nm propagates inside device A.

A maximum of 85% of power is transferred inside monitor 2 when wavelength 1550 nm propagates inside device A. The transmission graph in figure 16 (b) seem random and not depend on the number of defect pillars. This is because two pillars defect gave the most minimum power meanwhile the three single pillar give highest transmission.

The power that reflect back when wavelength 1550 nm propagates inside device is higher as shown in figure 16 (c). 78% of power is reflect back when the defect pillars inside the monitor is equal to two and five pillars.

From the investigation and analysis of the transmission characteristics when wavelength 1310 nm and 1550 propagates inside device A, an optimum design is proposed to split two wavelengths into two different output channels. The proposed design for splitting the wavelength 1310 nm and 1550 nm is using full defect pillars with diameter 124 nm in filter 1 and three pillars defect pillars with diameter of 285 nm in filter 2. With this design, it was found that it help to reduce reflectivity and boost up the power transmission in the device.
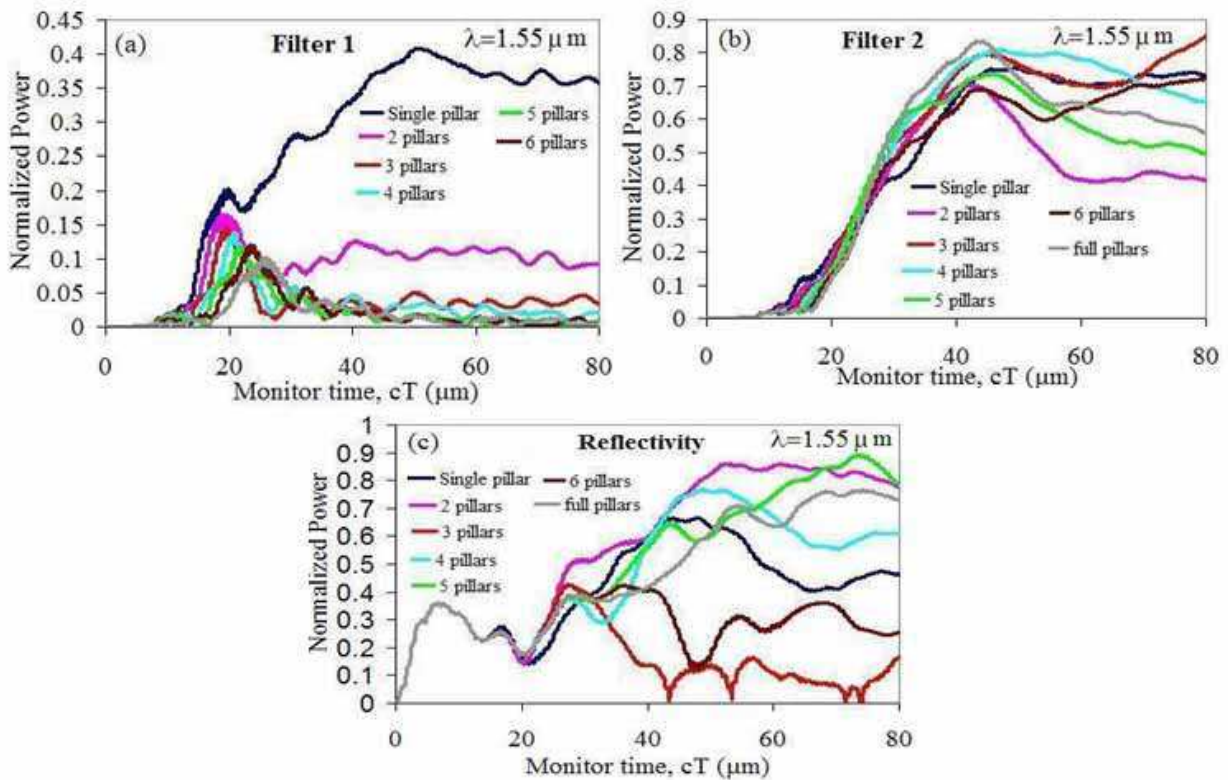
Fig. 16. Transmission characteristics inside filter 1, filter 2 and reflectivity when wavelength, λ of 1310 nm propagate inside device A.

The computed electromagnetic field distribution for device A is shown in Fig. 17 for two transmitted signals with wavelength 1310 nm (Fig. 17 (a)) and 1550 nm (Fig.17 (b)). Filter 1 has full defect pillars inside it and the diameter of defect pillars is smaller compare to diameter of surrounding pillars ($d_1<d$) in the left arm. The filter1 only permit wavelength
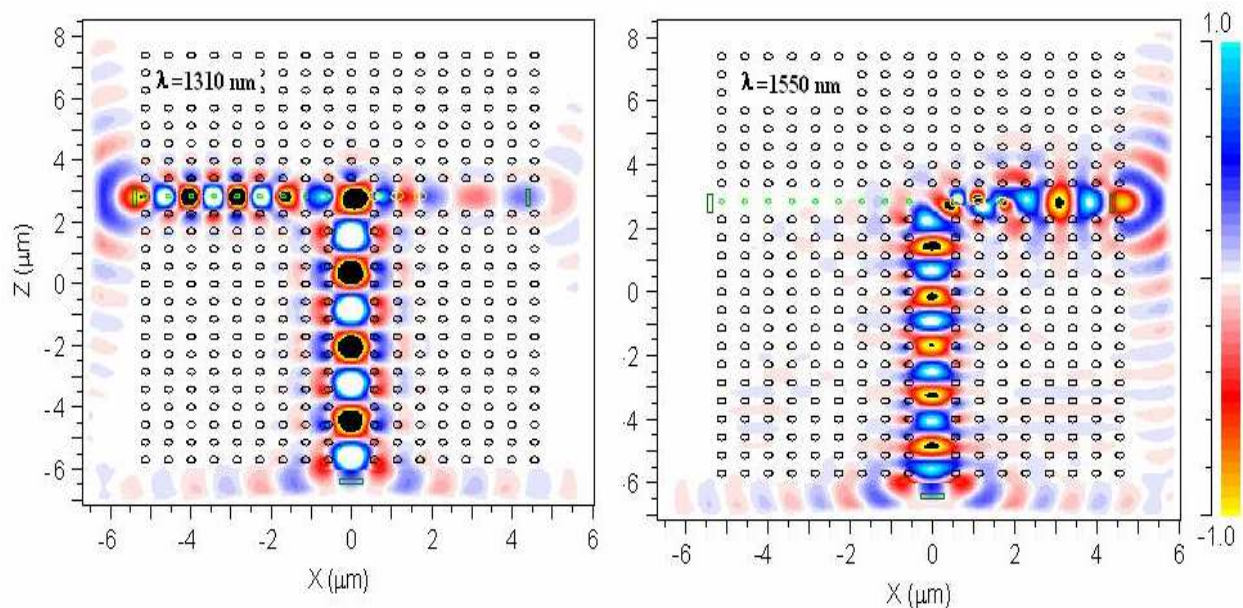
Fig. 17. Results of FDTD simulation of wavelength channel splitting for (a) source wavelength 1310 nm, and (b) source wavelength 1550 nm for device A

1310 nm to go through inside it and very small crosstalk was detected at monitor 2. Meanwhile filter 2 with diameter of defect pillars is bigger than the surrounding pillars ($d_2>d$) and three defect pillars inside it. Filter 2 in the right arm permit wavelength 1550 nm and reflects the wavelength of 1550 nm. Thus made the wavelength 1550 nm to turn to the left arm.

5.2 Device B: 1310 nm / 1550 nm demultiplexer/multiplexer based on Multimode Interference (MMI)

MMI based device is using the concept of interference phenomenon in it devices. Since the length of the device using an interference phenomenon is determined to be a common beat length for the multiple wavelengths, however, the device is quit long. To resolve this problem, in 2004, Kim et al. demonstrated that self imaging phenomenon also was valid in the PhC waveguide as well as in the dielectric waveguide (L.B. Soldano et al. 1995).

Self imaging is a property of multimode waveguides by which an input field profile is reproduced in a single or multiple images at periodic intervals along the propagation axis (L.B. Soldano et al. 1995). From the above definition, an input image can be reproduced in single or multiple images but, for the sake of simplicity, reproduction of only a single image is considered here. As shown in Fig.18, if an input field $\psi(0,y)$ is introduced into a multimode waveguide at $x=0$ with an asymmetric displacement d from the plane $y=0$, two kinds of images are reproduced at $x=L_m$ and $x=L_d$, depending on self-imaging conditions: one is a replica of the input field mirrored with respect to the plane $y=0$ at $x=L_m$ and the other is a direct replica of the input image at $x=L_d$.
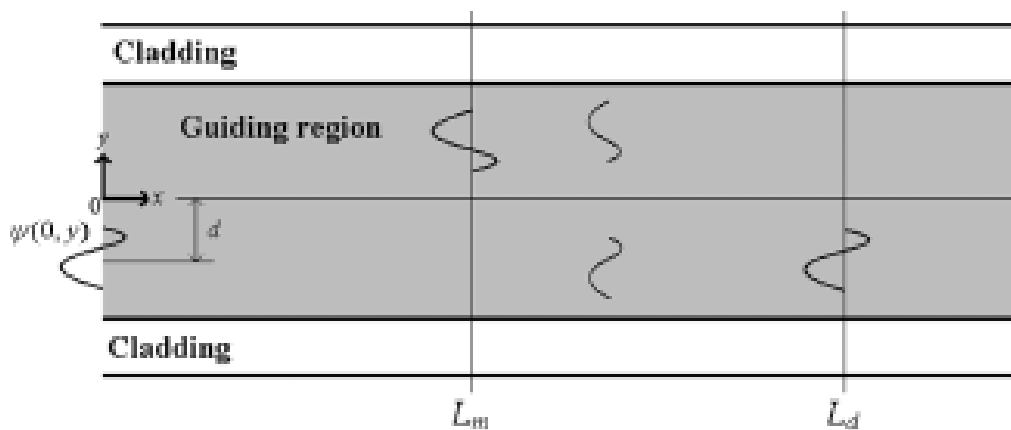

Fig. 18. Schematic illustration of a multi-mode waveguide. Input image is reproduced at $x=L_m$ and $x=L_d$.

For conventional waveguide, like the one presented above, self-imaging can be accepted without doubt or it may well be taken for granted. However, for a multi-mode PhC waveguide (PhCW), self imaging phenomena can still be observed. In order to prove that self imaging phenomena still valid in PhCW, a simulation which is similar to Fig.18 is simulate except that the conventional multi-mode waveguide is replaced with a PhC equivalent, as shown in Fig.19. In this structure, five consecutive rows are removed in otherwise perfect crystals to form a multi-mode PhCW.

As an access waveguide, a one-line defect PhCW is introduced into the multi-mode PhCW as shown in Fig.19. This access PhCW supports single-mode, and ensures that a well-confined input field is injected into the multi-mode PhCW for practical analysis.
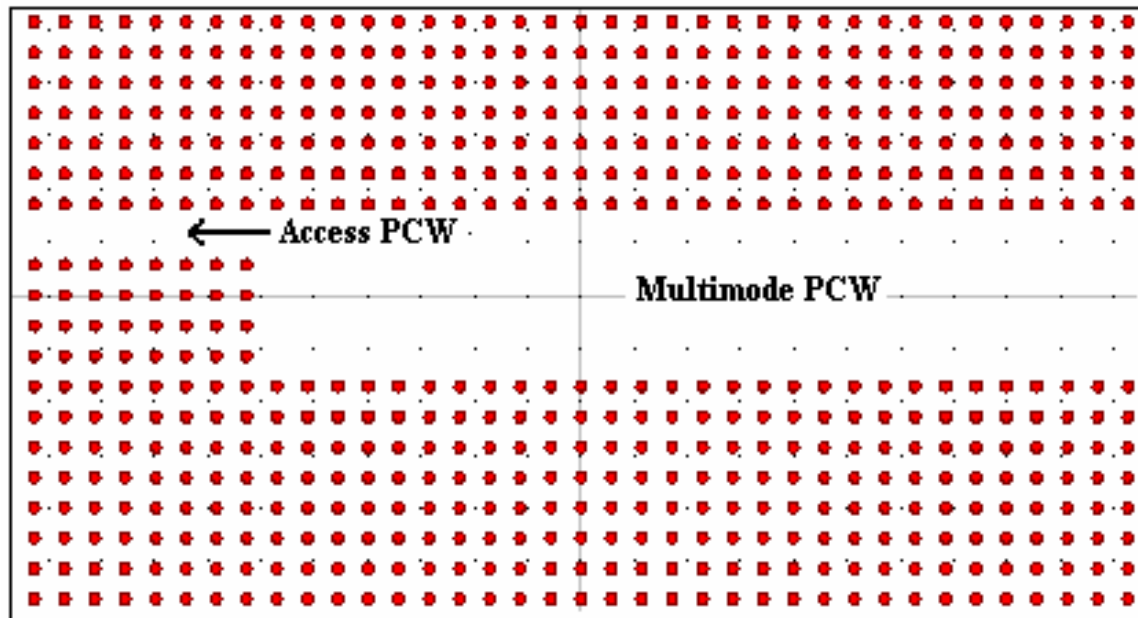
Fig. 19. Computational setup for observation of self imaging phenomena. The red dots represent dielectric rods (*n*=3.4) in air and their radius is 0.18*a*, where *n* is the refractive index of the rods and *a* is the lattice constant of the PhC.
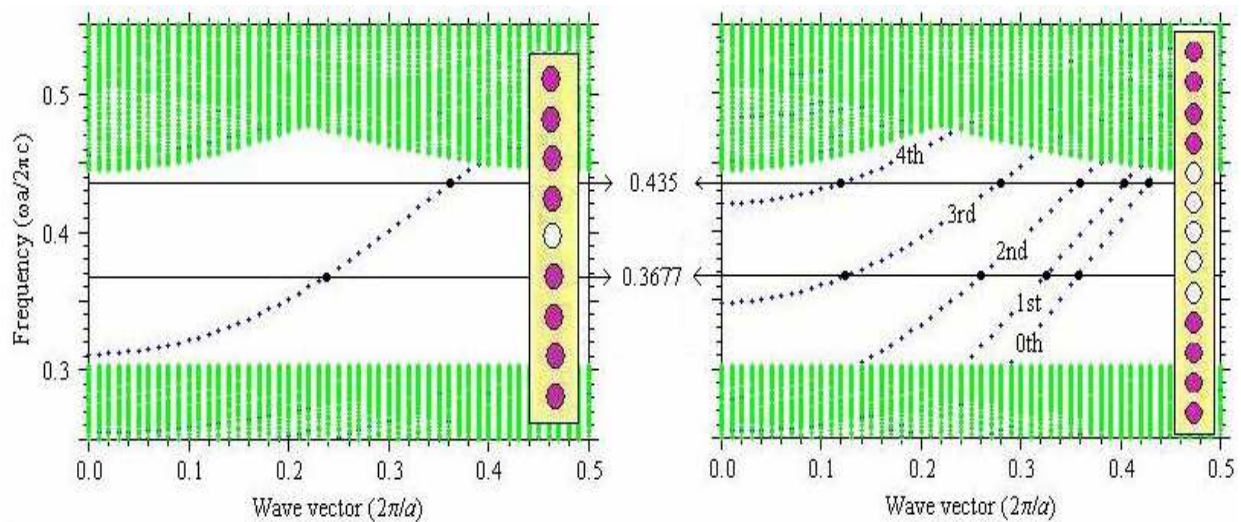

Fig. 20. (a) The dispersion curve for the access PhCW and the computational super-cell (inset). The access PhCW ensures single-mode operation from 0.312 (a/λ) to the top band gap. (b) The dispersion curve for the multi-mode PhCW and the computational super-cell (inset). The multi-mode PhCW supports 4 guided modes at $0.37(a/\lambda)$ and 5 guided modes at $0.43(a/\lambda)$

Before launching an input field into the multi-mode PhCW, the property of guided modes in the PCWs should be understand because self-imaging is attributed to the multi-mode interference, which strongly depends on the number of modes, propagation constants, and modal field patterns. To confirm the number of guided modes supported by the access PhCW and by the multi-mode PhCW, the dispersion curves for two PhCWs are presented in Fig. 20. The dispersion curves are calculated by the plane wave expansion (PWE) method.

In this crystal, the band gap opens for the frequency range of 0.303-0.445(a/λ) for *E*-polarization (electric field parallel to the pillars), where λ is the wavelength in free space. While the frequency range of single-mode operation for the access PhCW extends from 0.312(a/λ) to the top of the band gap, as shown in Fig.20 (a), the multimode-mode PhCW supports from three to five guided modes for the same frequency range (Fig.20(b)). In the frequency range, the operating frequency of 0.3677(a/λ) is chosen where the multi-mode PhCW supports more than three guided modes (higher than 0.35(a/λ)), as presented in Fig.20 (b).
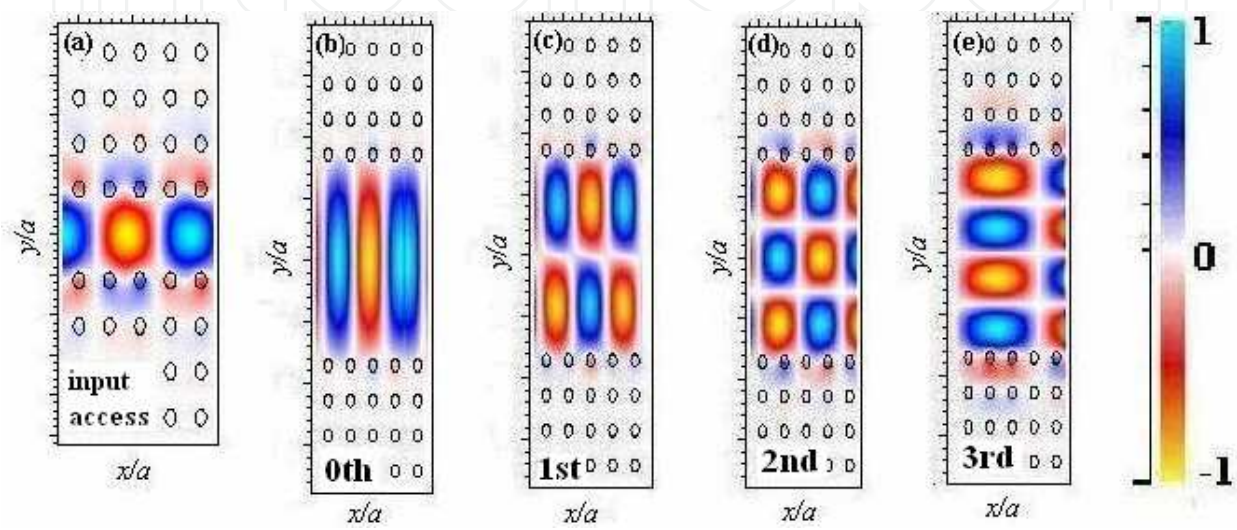

Fig. 21. Modal patterns of electric field in *z*-component for each mode at the operation frequency 0.37(a/λ) as presented in Fig.19. (a) Input image for access PhCW, (b) the 0th mode, (c) the 1st mode, (d) the 2nd mode, and (e) the 3rd mode at 0.37(a/λ).

To identify field patterns of guided modes in the access PhCW and the multi-mode PhCW, the modal field distribution are calculated at the opening frequency by the PWE method. Fig. 21 shows the *y*-component of the electric field at each calculation point, which are marked on dispersion curves in Fig. 20. The modal patterns have their own symmetry, even or odd, with respect to the propagation axis, hence the modal patterns can be selectively excited depending on the input position. However, in our case, since the access PhCW is introduced into the multi-mode PCW with an asymmetric position of *y*=2/*a*, as shown in Fig. 19, all the modes of the multi-mode PCW at the frequency of 0.37(a/λ) are excited by the input field (Fig. 20 (a)), which is confirmed by the overlap integral. Therefore, they all contribute to self-imaging.

The configuration of Fig. 19 is directly transferred to the FDTD computational domain for numerical experiment. The domain is surrounded by perfectly matched layers to absorb the outgoing waves. A continuous wave at the frequency of 0.37(a/λ) is launched into the access PhCW as shown in Fig. 22. The propagation shape inside the PhCW when 5 rows of pillar is removed is more likely to sinusoidal shape. It is likely that two kinds of images are reproduced by self imaging; one is expected to be mirrored replica at *x*=10*a* (L_m) and the other to be a direct replica at *x*=14*a* (L_d).
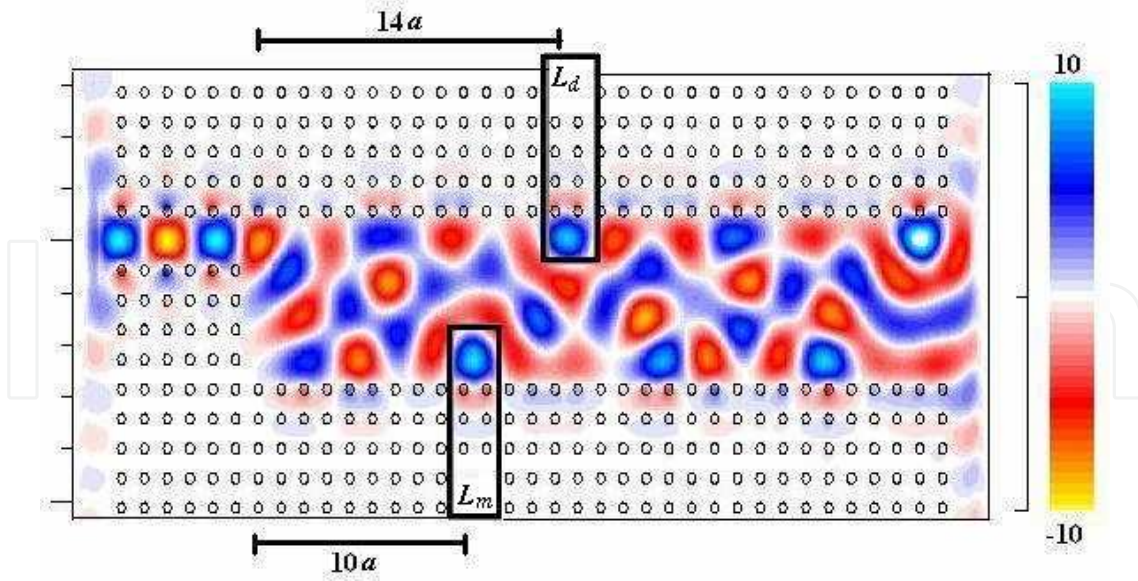
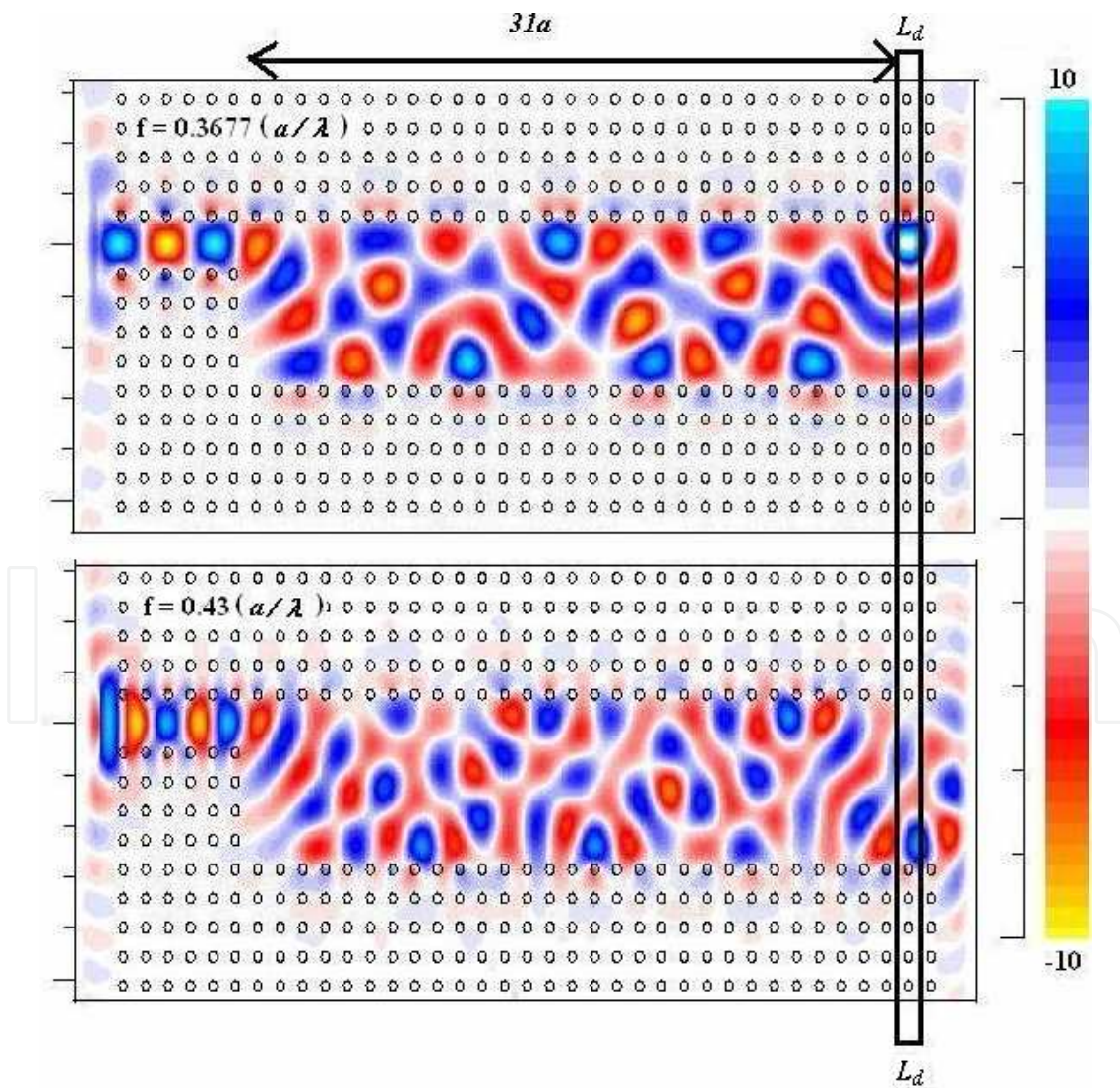Fig. 22. Steady-state electric field distribution at $0.3677(a/\lambda)$.

Fig. 23. Steady-state electric field distribution at $0.3677(a/\lambda)$ (*upper*) and at $0.43(a/\lambda)$ (*below*).

Fig. 23 shows steady-state electric field distribution at two different frequencies. As can be seen in both figures, the image inside the L_d box at $0.3677(a/\lambda)$ (upper) and at $0.43(a/\lambda)$ (below) is at different position but has same distant, L_d which is $31a$. From this picture, a DEMUX/MUX based on MMI can be designed. If arms are placed at $31a$, the two wavelengths can be guided inside two different output arms.

Fig. 24 shows a PhC DEMUX/MUX is designed by using self-imaging conditions. The objective is to separate two wavelengths (1310 nm and 1550 nm) so that a 1-to-2 structure is required for routing each wavelength to a corresponding output. As shown in Figure 23, two output PhCWs are added to the structure and the length, L_d of the multi-mode PhCW is set around $31a$, since the direct replica at $0.3677(a/\lambda)$ and $0.43(a/\lambda)$ are imaged at that position.
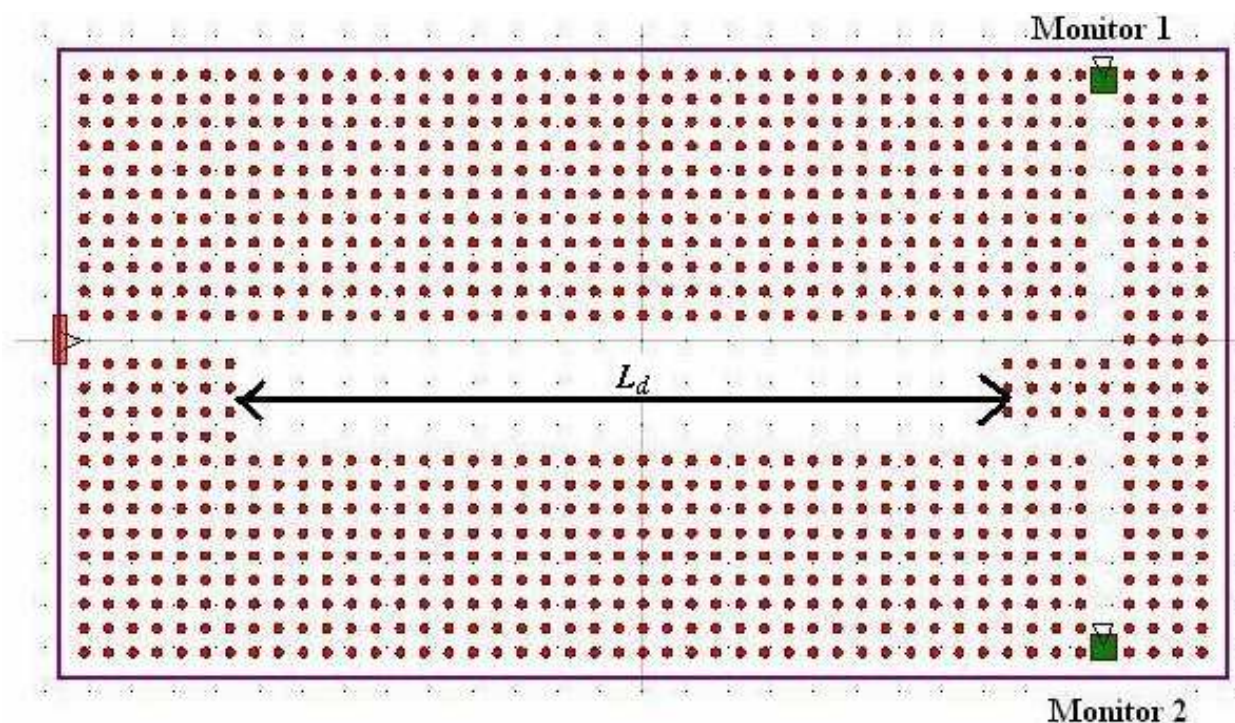

Fig. 24. The designed PhCW DEMUX/MUX MMI based.

This wavelength at $0.3677(a/\lambda)$ is intended to be routed to output port 1. Scanning computation of several frequency points on dispersion curves in Fig. 20 (b) makes it possible to determine another appropriate operating point of $0.43(a/\lambda)$ at which a mirrored replica is image at almost the same position as the direct replica is imaged (Fig. 23).

This design is directly applicable to a 1550/1310 nm DEMUX/MUX by setting the lattice constant, a, as 570nm. Unlike the previous situation at $0.37(a/\lambda)$, here there are five guided modes at $0.43(a/\lambda)$ to be considered-one more guided mode than at $0.37(a/\lambda)$, as shown in Fig. 20. However, the 4th mode is not excited, since it has odd symmetry with respect to the input field. Hence, four out of five modes are considered. Table 20 shows the final design parameters for device B with optimize value of L_m

Fig. 25 shows the steady-state electric field distributions as obtained by FDTD calculations after continuous waves at λ =1550 nm (Fig. 25 (left)) and λ=1310 nm (Fig.25 (right)) are launched into the access PhCW.

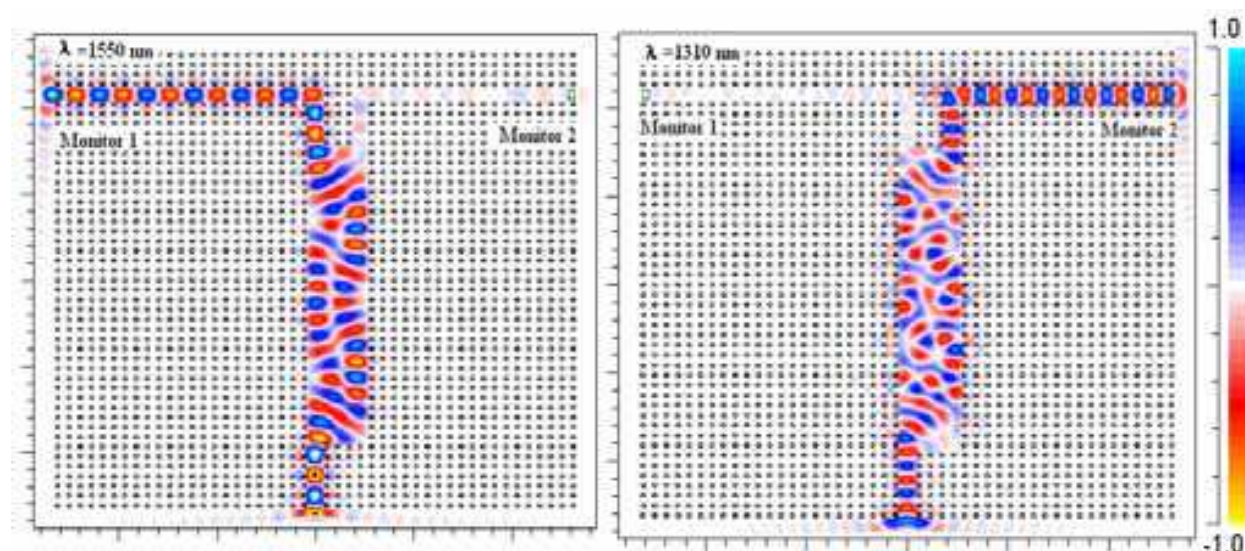Fig. 25. Steady-state electric field distributions in the designed PhC wavelength DEMUX/MUX MMI based at 1550 nm (*left*) and at 1310 nm (*right*).

6. Conclusion

Several of frailty has been identified in designing the DEMUX/MUX in PhC. For example, the power transfer inside the device not transfers 100% at the output arms. Light propagates inside the devices might dissipate along the waveguide. To minimize this losses, the design need to be alter, such as incorporate the defect pillar inside the space between two pillars so that the light will reflect back when the light incident with the defect pillar.

Development of planar lightwave circuit (PLC) devices by combining the conventional waveguides and PhCW need to be study. One of the mechanisms how to minimize the coupling loss between conventional waveguide and PhCW is by introduces taper waveguide at the end of PhCW. By introducing taper waveguide, the bigger spot size from conventional waveguide will slowly shrink when enter the taper waveguide at the PhCW.

Most of the work in this thesis focuses on optical communication PLC technology. Application area of photonic crystal devices can be extends into other applications. PhC can also be implemented in other applications such as bio-sensing, imaging, illumination, etc. The investigation on how the existing devices can be used for such applications and new devices/materials will have to be developed to address these areas.

In the future, PhC components will by widely used in optical telecommunications. Since the invention of the concept of PhC in the end of of the 80's, their properties have been studied intensively. New applications have been proposed and realized. The only components that are so far in commercial use are the photonic crystal fibers. They have many extraordinary properties that cannot be achieved using conventional fibers and thus will have a profound effect on the fiber optics industry. In the near future, other PhC components, such as fiber lasers, will also be brought into market.

7. References

B. S. Song, S. Noda and T. Asano, 2003. *Science,* 300: 1537.
B. S. Song, S. Noda, T. Asano and Y. Akahane, 2005, *Nature Materials,* 2: 207.

Baba T., & Matsuzaki T. 1996. Fabrication and photoluminescence studies of GaInAs/InP 2-dimensional photonic crystals. *Japanese Journal of Applied Physics, Part 1 (Regular Papers & Short Notes)* 35(2B): 1348-1352.

Baba T., Inoshita K., Tanaka H.,Yonekura J., Ariga M., Matsutani A., Miyamoto T., Koyoma F. & Iga K. 1999. Strong enhancement of light extraction efficiency in GaInAsP 2D arranged microcolumns. *Journal of Lightwave Technology* 17(11):2113-2120.

Benisty H., Weisbuch C., Labilloy D., Rattier M., Smith C. J. M., Krauss T. F., de la Rue R. M., Hourde R., Oesterle U., Jouanin C.& Cassagne D. 1999. Optical confinement properties of two-dimensional photonic crystals. *Journal of Lightwave Technology* 17(11): 2063-2077.

Boroditsky M., Gontijo I., Jackson M., Vrijen R. Yablonovitch E., Krauss T., Chuan Cheng Cheng, Scherer A., Bhat R. & Krames M. 2000. Surface recombination measurements on III-V candidate materials for nanostructure light-emitting diodes. *Journal of Applied Physics.* 87(71): 3497-3504.

C. Manolatou, S. G. Johnson, S. Fan, P. R. Villeneuve, H. A. Haus & J. D. Joannopolous. 1999. High-density integrated optics. *IEEE J. Lightwave Technol.* 17: 1682-1692.

C. T. Lee & M. L. Wu. 2001. Apaxes-linked circle gratings for low-loss waveguide bends. *IEEE Photon. Technol. Lett* 13: 597-599.

Chul-Sik Kee, Jae-Eun Kim and Hae Yong Park. 1997. Absolute photonic band gap in a two-dimensional square lattice of square dielectric rods in air, *Rapid Communications Physical Review E*, Volume 56, number 6.

Chutinan A.& Noda S. 1999. Highly confined waveguides and waveguide bends in three-dimensional ph otonic crystal. *Applied Physics Letters.* 75(24): 3739-3741

Cregan R. F., Mangan B. J., Knight J. C., Birks T. A., Russell P. St. J., Roberts P. J. & Allan D. C. 1999. Size-mode photonic band gap guidance of light in air. *Science* 285(5433):1537-1539.

D. K. Armani, T. J. Kippenberg, S. M. Spillane and K. J. Vahala. 2003. Ultra-high-Q toroid microcavity on achip. *Nature* 421, 925-928.

D. L. Lee. 1986. *Electromagnetic principles of integrated optics* New York: John Wiley & Sons.

D. W. Vernooy, V. S. Ilchenko, H. Mabuchi, E. W. Streed, and H. J. Kimble. 1998. High-Q measurements of fused-silica microspheres in the near infrared. *Opt. Lett.*23, 247-249.

Djafar K., Mynbaev & Lowell L. Scheiner. 2001. Fiber-optic communications Technology New York: Prentice Hall

Eli Yablonovitch & T. J. Gmitter. 1991. Photonic band structure: the face centered cubic case employing nonspherical atoms. *Physical Review Letters* 67: 2295-2298.

Eli Yablonovitch. 1987. Inhibited spontaneous emission in solid State physics and electronics. *Physical Review Letters* 58: 2059-2062.

H. Nishihara, M Haruna & T. Suhara. 1989. *Optical integrated circuits*. New York: McGrawHill.

J. S. Foresi, P. R. Villeneuve, J. Ferrara, E. R. Theon, G. Steinmeyer, S. Fan, J.D. Joannopolous, L.C. Kimerling, H.I. Smith and E. P. Ippen, 1997, *Nature*, 390: 143.

K. Inoue & K. Ohtaka. 2004. *Photonic crystals: physics, fabrication and applications.* New York: Springer-Verlag Berlin Heidelberg.

K. M. Ho., C. T. Chan & C. M. Soukoulis. 1990. Existance of a photonic band gap in periodic dielectric structures. *Physical Review Letters* 65: 3152-3155.

K. M. Leung & Y. F. Lin. 1990. Full vector wave: calculation of photonic band structures in face centered cubic dielectric media.

K. Okomoto. 1999. *Integrated optical circuits and components: Design and applications*. New York: Marcel Dekker.

Knight T C., Birks T. A., Russell P. St. J. & de Sandro J. P. 1998. Properties of photonic crystal fiber and effective index material. *Journal of the Optical Society of America A (Optics, Image Science and Vision)* 15(3): 748-752.

Kosaka H., Kawashima T., Tomita A. Notomi M., Tamamura T., Sato T. & Kawakami S. 1998. Superprism phenomena in photonic crystals. *Physical Review B (Condensed Matter)* 58(1615): R10096-R10099.

Kristina Grifantini, 2008Nature's Photonic Crystal, Scientists find an elusive diamond structure in a Brazilian beetle. *Technology Review published by MIT*. www.technologyreview.com/Nanotech/20840/?nlid=1115&a=f

L.B. Soldano et al., 1995. Optical multi-mode interference devices based on self-imaging: principles and applications. *J. Lightwave Technol.* 13, 615-627.

M. Koshiba 1992. *Optical waveguide analysis*. New York:McGraw-Hill

M. Popovic, K. Wada, S. Akiyama, H. A. Haus & J. Miche. 2002. Air trenches for sharp silica waveguide bends. *J. Lightwave Technology* 20:1762-1772.

Mekis A., Chen J. C., Kurland I., Fan S., Villeneuve P. R. & Joannopolous J. D. 1996. High transmission through sharp bends in photonic crystal waveguides. *Physical Review Letters.* 77(18): 3787-3790.

O. Painter, R. K. Lee, A. Scherer, A. Yariv, J. D. O'Brien, P. D> Dapkus, and I. Kim, 1999, *Science*, 284: 1819.

O'Brien J., Painter O., Lee R., Cheng C. C., Yariv A., & Scherer A. 1996. Laser incorporating 2D photonic bandgap mirrors. *Electronics Letters.* 32(24): 2243-2244.

Ohtera Y., Sato T., Kawashima T. Tamamura T.& Kawakami S. 1999. Photonic crystal polarization splitters. *Electronics Letters* 35(15): 1271-1272.

Pete Vukusic & J. Roy Sambles. 2003. Photonic structures in bilogy. *Nature* 424(680): 852-855.

R. A. Jarvis, J. D. Love & F. Ladouceur. 1997. Bend-radius reduction in planar waveguide using UV post-tuning. *Electron Lett.*33:892-894.

R. Colombelli, K. Srinivasan, M. Troccoli, O. Painter, C. F. Gmacgl, D. M. Tennant, A. M. Sergent, D. L. Sivco, A. Y. Cho and F. capasso, 2003, *Science*, 302: 1374.

R. L. Espinola, R. U. Ahmad, F. Pizzuto, M. J. Steel & R. M. Osgood. 2001. A study of high-index contrast 90 degree waveguide bend structures. *Opt Express.* 8:517-528.

S. Lardenois, D. Pascal, L. Vivien, E. Cassan & S. Laval. 2003. Low-loss submicrometer silicon-on-insulator rib waveguides and corner mirrors. *Opt. Lett.* 28:1150-1152.

S. Noda, A. Chutinan and M. Imada, 2000. *Nature*, 407:608.

S. Ogawa, M. Imada, S. Yoshimoto, M. Okano and S. Noda, 2004. *Science*, 305: 227.

S. Y. Lin, V. M. Hietala, S. K. Lyo, and A. Zaslavsky, 1996, *Appl. Phys. Lett.*, 68,3233

Sajev John. 1987 Strong localization photon in certain disordered dielectric superlattices. *Physical Review Letters.* 58:2486-2489. *Physical Review Letters* 65: 2646-2649.

Shanshui Fan, Villeneuve P. R., Joannopolous J. D. & Schubert E. F. 1997. High extraction efficiency of spontaneous emission from slabs of photonic crystals. *Physical Review Letters.* 78(17): 3249-3247.

Y. Akahane, T. Asano, B. S. Song and S. Noda, 2003, *Nature*, 425: 944.

Yablonovitch E., Gmitter T. J., Meade R. D., Rappe A. M., Brommer K.D. & Joannopolous J.D. 1991. Donor and acceptor modes in photonic band structures. *Physical Review Letters* 38 (249): 3380-3383.

Yonekura J., Ikeda M.& Baba T. 1999. Analysis of finite 2D photonic crystals of columns and lightwave devices using scattering matrix method. *Journal of Lightwave Technology* 17(8): 1500-1508.
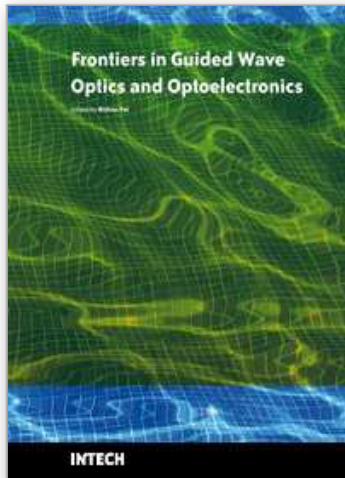
Frontiers in Guided Wave Optics and Optoelectronics

Edited by Bishnu Pal

As the editor, I feel extremely happy to present to the readers such a rich collection of chapters authored/co-authored by a large number of experts from around the world covering the broad field of guided wave optics and optoelectronics. Most of the chapters are state-of-the-art on respective topics or areas that are emerging. Several authors narrated technological challenges in a lucid manner, which was possible because of individual expertise of the authors in their own subject specialties. I have no doubt that this book will be useful to graduate students, teachers, researchers, and practicing engineers and technologists and that they would love to have it on their book shelves for ready reference at any time.

How to reference

In order to correctly reference this scholarly work, feel free to copy and paste the following:

Sahbuddin Shaari and Azliza J. M. Adnan (2010). Photonic Crystal Multiplexer/Demultiplexer Device for Optical Communications, Frontiers in Guided Wave Optics and Optoelectronics, Bishnu Pal (Ed.), ISBN: 978-953-7619-82-4, InTech, Available from: http://www.intechopen.com/books/frontiers-in-guided-wave-optics-and-optoelectronics/photonic-crystal-multiplexer-demultiplexer-device-for-optical-communications

INTECH
open science | open minds